The Autopalmitoylated Vesicular Transport Protein Bet3:

Biochemical and Fluorescence-based Characterization of Membrane and Substrate Binding

Inaugural-Dissertation
to obtain the academic degree
Doctor rerum naturalium (Dr. rer. nat.)

submitted to the Department of Biology, Chemistry and Pharmacy
of Freie Universität Berlin

by

Julia Elsbeth Ingeburg Walter

from Göttingen

Berlin 2017

Die praktischen Arbeiten für diese Dissertation fanden im Zeitraum von Juni 2007 bis Dezember 2010 am Institut für Immunologie und Molekularbiologie (IMB) der Freien Universität Berlin unter der Betreuung von PD Dr. Michael Veit statt.

1. Gutachter: Prof. Dr. Udo Heinemann
2. Gutachter: PD Dr. Michael Veit

Disputation am 12.07.2017

Danksagung

Bei meinen Doktorvätern, PD Dr. Michael Veit und Prof. Dr. Udo Heinemann, bedanke ich mich für die Überlassung des Themas, ihre Unterstützung, die guten Ratschläge und die hilfreichen fachlichen Diskussionen während meiner Promotionszeit. Ein ganz besonderer Dank auch dafür, dass sie mir nach krankheitsbedingter Pause die Chance gegeben haben meine Promotion doch noch abzuschließen.

Besonders erwähnen möchte ich unsere Technischen Assistentinnen Frau Poese und Frau Palissa sowie unsere Sekretärin Frau Daberkow, die durch ihre organisatorische Unterstützung unser Labor am Laufen gehalten und mir erst meine Arbeit ermöglicht haben.

Ein ganz besonderer Dank gebührt meinem Kollegen Dr. Bastian Thaa, der mir nicht nur Freund und gar nicht genug geschätzter Gesprächspartner ist, sondern auch meine Dissertation gegengelesen und durch seine Anregungen zu ihrer Verbesserung beigetragen hat.

Ebenso gilt mein Dank all meinen weiteren Kollegen, so wie meiner Familie und meinen Freunden, die mir immer zur Seite gestanden haben.

TABLE OF CONTENTS

1 Introduction

1.1 TRAPP and vesicular transport

Eukaryotic cells are not only surrounded by the lipid bilayer of the plasma membrane, but also divided by lipid membranes into different compartments, called organelles. Because of their hydrophobic nature these membranes separate the inside of the organelles from the cytosol and allow for distinct composition of each organelle's interior suited to its special task, such as protein synthesis in the endoplasmic reticulum (ER) or protein sorting and maturation in the Golgi apparatus. To maintain the distinction between organelles, the transport of proteins across the lipid bilayers as well as the exchange of proteins between organelles is strictly controlled.

In eukaryotic cells the transport along secretory and endocytic pathways is performed by vesicular carriers. Vesicles bud from one compartment, taking along both soluble and membrane proteins as well as lipids, and fuse with the organelle membrane of their destination (see fig.1.1).

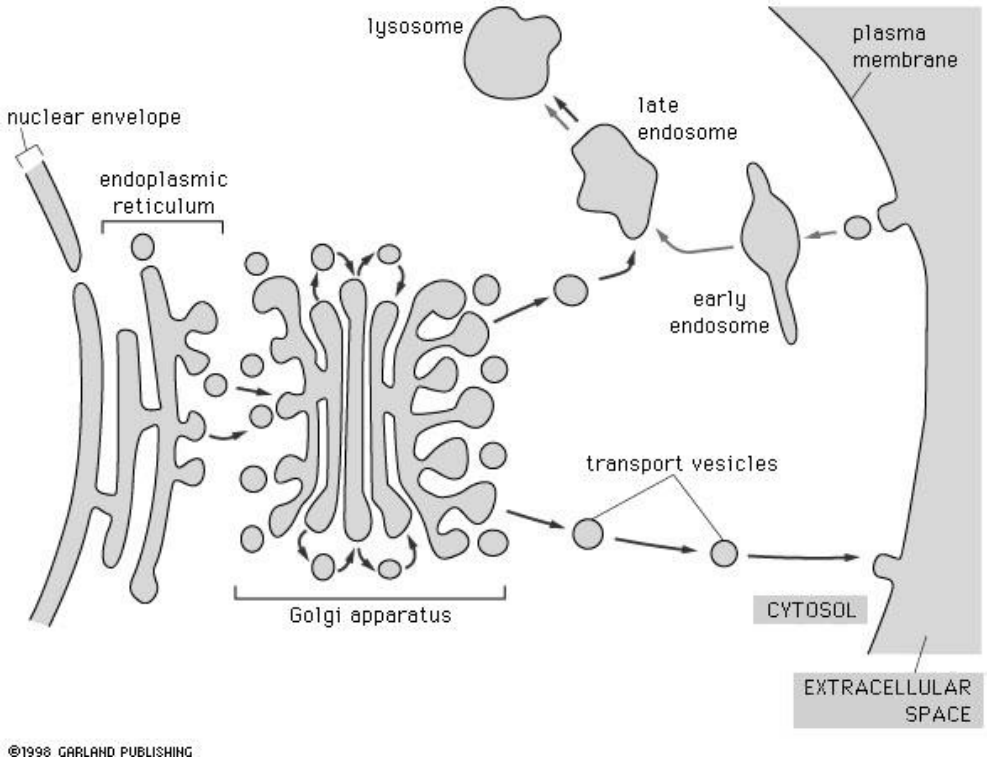

(Alberts, B., Essential cell biology: an introduction to the molecular biology of the cell, 1998)

Figure 1.1: Schematic diagram of inner cellular vesicle transport [1]. Membrane proteins or proteins destined for exocytosis are transported in vesicles from the ER to the Golgi, where they are modified and sorted. From the Golgi they are either transported to the plasma membrane or to the late endosome and on to the lysosome.

Budding is driven by the assembly of coat proteins on the membrane surface of the origin compartment. They bind proteins to sort them into the budding vesicle, induce membrane curvature and eventually pinch off the new vesicle. The anterograde transport between ER and Golgi is mediated by COPII (coat protein complex II) coated vesicles, whereas retrograde transport, which recycles the components of the transport machinery back to the ER, occurs in COPI coated vesicles.

Proteins mediating the recognition between vesicles and their target membranes and effectuating the initial attachment of the vesicle are called tethers. At the Golgi the initial tether is a TRAPP (transport protein particle) complex. Besides acting as tethers, TRAPP complexes also act as a guanidine exchange factor (GEF) for the GTPase Ypt1p/Rab1 [2-4]. The GTPase is activated by TRAPP and recruits an additional tether (the coiled-coil protein Uso1p/p115) to the Golgi membrane [5]. This tether then promotes the formation of a SNARE (soluble N-ethylmaleimide-sensitive-factor attachment receptor) protein complex which initializes membrane fusion [6]. The targeting of the vesicle to the correct compartment and the subsequent membrane fusion are tightly regulated events.

To date three TRAPP complexes have been identified. TRAPP I, composed of seven subunits, is required for vesicular ER-to-Golgi transport and binds specifically to ER-derived transport vesicles [7, 8] (see fig. 1.2). The subunit Bet3 is present twice in the complex and it is thought that TRAPP performs its tethering function by interaction of Bet3 with the vesicles coat proteins on one side and the organelle membrane on the other [4]. In yeast TRAPP is tightly associated with the Golgi membrane, where it mediates the fusion of COPII coated vesicles with the *cis*-Golgi [7].

Mammalian TRAPP is less tightly bound and partly exists as unassembled cytosolic proteins [9]. In mammalian cells TRAPP I interacts via its Bet3 subunit with the Sec23 subunit of the vesicle's COPII coat which leads to their homotopic fusion to form an intermediate compartment (IC) [10]. The IC is a distinct cluster of tubular membranes located between ER and Golgi and is thought to function as an additional protein sorting compartment [11].

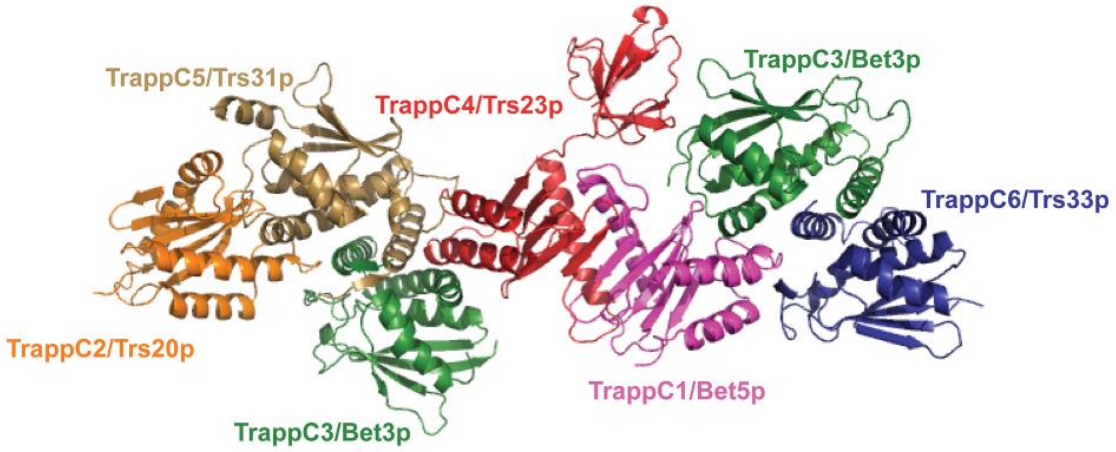

(Brunet et al., In sickness and in health: the role of TRAPP and associated proteins in disease. Traffic,2014)

Figure 1.2: The seven subunits of the TRAPP I complex with the yeast and mammalian nomenclature [12]. Bet3 (green) is present twice, located towards the ends of the complex.

TRAPP II is involved in trafficking between the *trans*-Golgi and early endosome and consist of TRAPP I plus three additional subunits [8, 12]. TRAPP III is located at the phagophore and necessary for autophagy. It is composed of TRAPP I plus one additional subunit [13]. Malfunctions of the TRAPP complexes are involved in cancer, growth impairment and neurological diseases [14].

1.2 The TRAPP subunit Bet3 contains covalently bound palmitate

In this work human Bet3, also termed TrappC3, has been used. Since most findings about Bet3 stem from experiments with the yeast homolog, the name Bet3 will be used throughout this work for convenience. Bet3 is the best conserved subunit of the TRAPP complex showing a 54 % sequence identity between yeast and human [15]. Bet3 is ubiquitously expressed, but unlike other TRAPP subunits, there are to date no diseases associated with mutations in Bet3. It is quite likely that Bet3 is so essential to the protein transport inside the cell, that a mutation would be embryotic lethal.

The crystal structure of Bet3 shows four antiparallel β-strands and four α-helices in an α/β-plaid fold (see fig. 1.3). A hydrophobic tunnel spans the protein, with an approximate length of 20 Å. It is formed by the C-terminal end of α2, the loop connecting α2 and α3 and the helices α3 and α4. The amino acids lining the tunnel are highly conserved. At the entrance to the tunnel a fully conserved cysteine (C68) is located, on which a palmitate chain is covalently attached via a thioester bond [16]. The exact function of the palmitate chain is as yet not fully understood, since yeast cell viability tests showed

that while Bet3 is essential, the palmitoylation of Bet3 is not critical for localization or function *in vivo* [17]. However lack of palmitoylation increases the inherent instability of Bet3 [18].

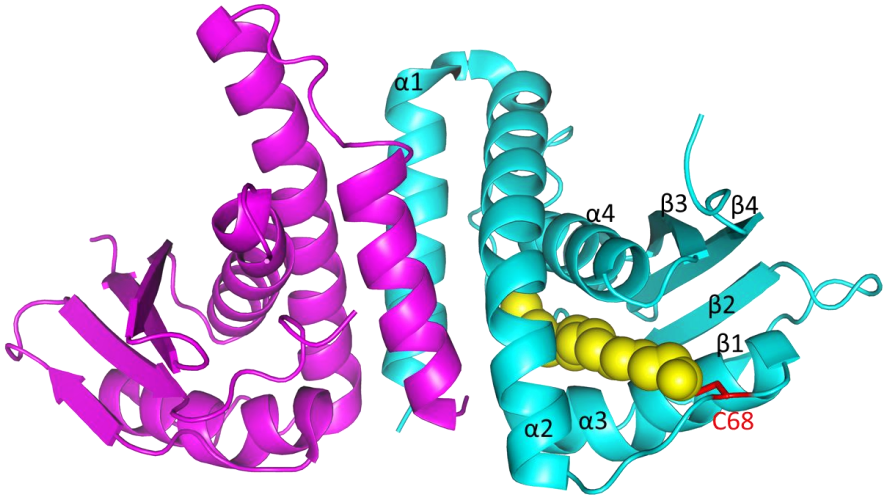

Figure 1.3: Cartoon of the Bet3/TrappC6 heterodimer. Bet3 (cyan) consist of four antiparallel β-strands and four α-helices folded in an α/β-plaid fold. The protein has a hydrophobic tunnel formed by highly conserved residues in which a palmitoyl moiety (yellow) covalently attached to C68 is embedded. In the TRAPP complex Bet3 interacts with TrappC6 (pink) with which it can be co-purified as a heterodimer. The cartoon of the protein structure was generated with PyMol, pdb 2CFH.

1.3 Mechanism of palmitoylation of Bet3

Palmitoylation of proteins can perform several functions. It can serve as a sorting and trafficking signal determining the localization to cellular membranes, most often to the plasma membrane, but also to other organelles [19]. It is also believed that palmitoylation of transmembrane proteins facilitates their association with lipid rafts, membrane areas of high cholesterol content, which causes denser lipid packing and decreased fluidity of the lipid bilayer. The preferred association with lipid rafts was also observed for some palmitoylated peripheral proteins, like e.g. members of the Ras GTPase family [19, 20]. However this effect could not be shown for all transmembrane proteins and the exact mechanisms of raft localization remain to be elucidated [20]. For many proteins palmitoylation is a dynamic modification, with cycles of palmitoylation and de-palmitoylation allowing for the movement of proteins between organelles or in and out of raft domains. Palmitoylation also has been shown to increase protein stabilization, either by preventing their ubiquitylation, a signal for protein degradation, or simply by suppressing protein aggregation [20].

Palmitoylation of proteins is normally conveyed by DHHC S-acyl-transferases, a family of enzymes characterized by a cysteine-rich domain with a DHHC (Asp-His-His-Cys) motive. DHHC proteins probably palmitoylate their substrates by first becoming themselves auto-acylated by palmitoyl coenzyme A (Pal-CoA) and then transferring the palmitate chain [21, 22].

The most striking feature of Bet3 is, that it does not need DHHC S-acyltransferases for palmitoylation, as could be shown by expression of Bet3 in yeast strains defective for members of the DHHC protein family. Furthermore, Bet3 purified from *E. coli*, which lack DHHC proteins and therefore are not able to acylate proteins, also contains covalently bound palmitate [23]. Instead it is able to catalyze its own palmitoylation with Pal-CoA as substrate via a bimolecular nucleophilic substitution (S_N2) mechanism at C68. Incubation of purified Bet3 wild-type with [^{3}H]-Pal-CoA showed that the reaction has a broad pH optimum at neutral pH (pH 6.5-8.5), but is inhibited at acid pH and strongly reduced at basic pH. Pal-CoA is capable of spontaneously acylating free cysteines, but this non-catalytic reaction would show even higher efficiency at basic pH. So the decrease in palmitoylation at high pH is a strong indicator of catalytic activity. The apparent K_m of 5.7 µM lies within the physiological concentration range of Pal-CoA inside cells [18, 24].

The residue arginine 67, neighboring the acylation site, is also highly conserved. The side chains of R67 and C68 are 7.2 Å apart, so that R67 cannot directly deprotonize C68's sulfhydryl group. It probably aids the S_N2 reaction by decreasing the pK_a of the cysteine through electrostatic interactions and stabilizing the negative charge of the reaction intermediate. The supportive function was proven by palmitoylation assays with a R67E mutant, showing only weak and retarded palmitoylation at physiological pH [18, 25].

In the Bet3 mutant A82V the hydrophobic tunnel is partly blocked by the valine. The mutant showed no palmitoylation at physiological pH, indicating that insertion of the fatty acid is a requirement for the autocatalytic reaction [18, 25]. As virtually all cytosolic acyl-CoA is bound by the cytosolic acyl-CoA binding protein (ACBP) and therefore not available [24], the sole source of acyl-CoAs as substrates for the autopalmitoylation reaction are acyl-CoAs embedded in organelle membranes. Since Bet3 resides on the membrane surface and is not embedded in the lipid bilayer the question remains if the tunnel binding site is sufficient to extract membrane integrated acyl-CoAs.

Attempts to co-crystalize Bet3 C68A with Myr-X-CoA (a non-hydrolysable Pal-CoA substitute) and thus to exactly describe the substrate binding site were unsuccessful [25]. Therefore, in this work an indirect characterization of the substrate binding site is attempted through fluorescence quenching assays with purified Bet3. It has been shown that Bet3 can be acylated by different acyl-CoAs but the binding constants of acyl-CoAs of different length and shape still needed to be determined. Also the hypothesis that the hydrophobic tunnel is the substrate binding site was tested using different Bet3 mutants.

1.4 Mechanism of membrane binding of Bet3

Bet3 is thought to mediate membrane binding of the TRAPP complex, so that TRAPP can fulfill its role as tether. In yeast its localization on the Golgi and stable membrane binding could be shown [3]. In mammalian cells only about 15 % of Bet3 are tightly membrane bound, the remainder is cytosolic [9].

Several possible mechanisms for the interaction between Bet3 and the lipid bilayer have been suggested. Firstly, the covalently bound fatty acid could insert itself into the membrane (see fig. 1.4 A). Secondly a fatty acid chain from the membrane could insert itself into the tunnel (see fig. 1.4 B). Both possibilities would require twisting of the palmitoyl chain out of the hydrophobic tunnel.

Based on structural similarities with the barley lipid transfer protein (LTPs), it has been proposed that the palmitate moiety could extend from the hydrophobic tunnel, if the helix α2 would undergo a 30° rotation to open the lipid binding pocket [16]. This would allow for interaction with the lipid bilayer of membranes or other interaction partners through either the palmitate chain or by intrusion of another hydrophobic moiety into the now empty tunnel.

Thirdly the homodimer of Bet3 shows a large flat surface with a patch of conserved, positively charged residues (K13, R62, R67, K80 and K96). It has been suggested that membrane binding is mediated by electrostatic interaction between the positively charged planar surface of the Bet3 dimer (or the Bet3/TrappC6 hetero dimer of the TRAPP complex respectively) and the membrane surface (see fig. 1.4 C) [16, 17]. Fourthly binding might also occur through interaction with a protein in the organelle membrane (see fig. 1.4 D).

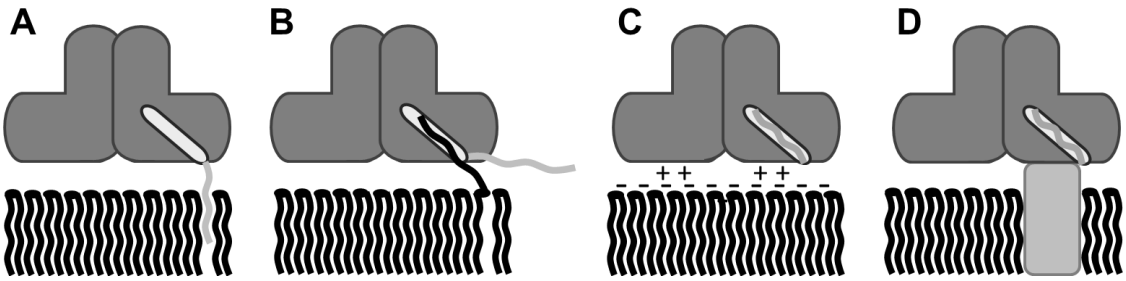

Figure 1.4: Proposed Bet3 membrane binding mechanisms: (A) By extrusion of the covalently bound fatty acid and its insertion into the membrane's lipid bilayer. (B) By insertion of a fatty acid from the membrane into the hydrophobic tunnel of Bet3. (C) By electrostatic interaction between the positively charged planar surface of the Bet3 dimer and negatively charged phospholipids in the membrane surface. (D) By interaction with a membrane bound protein.

Growth experiments with HA-tagged Bet3 mutants in a temperature sensitive yeast strain [17] showed that blocking of the hydrophobic tunnel (mutant A82L) and removal of the positive charges on the flat Bet3 surface (mutant K13E K84E) both were conditionally lethal and caused unspecific attachment to a variety of intercellular compartments (A82L) or completely inhibited membrane binding (KKEE), suggesting that insertion of a fatty acid in the tunnel, as well as electrostatic binding to the membrane were both involved in the specific attachment to the Golgi membrane. However repetition of the experiments with untagged Bet3 could not validate these results [4]. In neither experiment the suppression of palmitoylation showed an effect on membrane binding [4, 17].

The localization of Bet3 in a living cell changes with the different TRAPP complexes and might also be influenced by other factors, as can be seen by the conflicting results obtained by using Bet3 with and without HA tag. Therefore, the proposed membrane binding mechanisms, insertion of palmitate into the membrane or of a fatty acid in the hydrophobic tunnel or electrostatic interaction, were again investigated using purified Bet3 and artificial membranes.

1.5 Fluorescence

Since most data of this work was acquired using fluorescence spectroscopic techniques the basic theories of fluorescence, tryptophan quenching and fluorescence anisotropy are introduced below. The following two chapters are based on the *Principles of fluorescence spectroscopy* by J. R. Lakowicz [26].

The emission of light upon the return of an electron from an electronically excited state to its ground state is called luminescence and can be divided in fluorescence and phosphorescence depending on the nature of the excited state. Fluorescence is the return from an excited singlet state to the singlet ground state. In the excited singlet state the electron's spin is paired to the one in the ground state, so that the return to the ground state occurs with high probability. Therefore, the fluorescence lifetime is short, in the range of nanoseconds. Phosphorescence on the other hand, is the return from a triplet state, in which the excited electron has the same spin orientation as the ground state. Return to the ground state requires a "forbidden" spin inversion and is therefore less likely. In consequence the lifetime of the excited state can range between milliseconds and hours. Because the return to the ground state always occurs from the lowest excited state, the emission is always shifted to longer wavelength compared to the excitation (Stokes shift). The different processes involved in the absorption and emission of light can be visualized in a Jablonski diagram (see fig. 1.5)

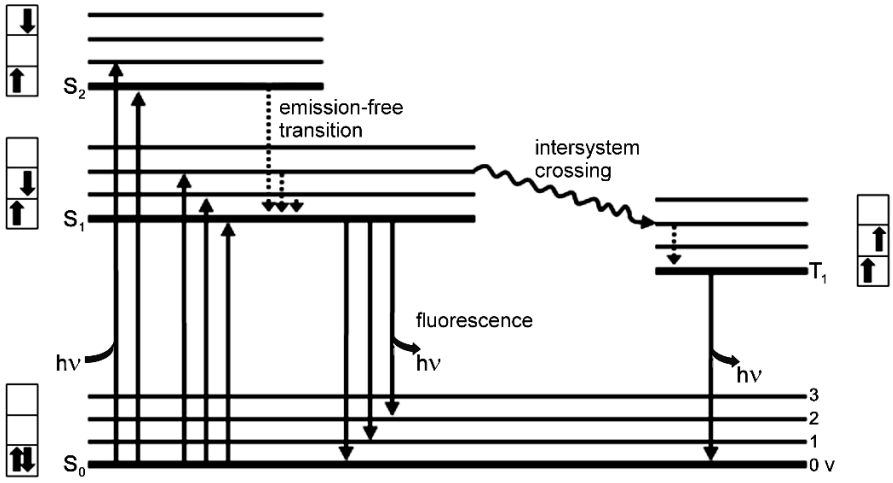

Figure 1.5: Jablonski diagram: Excitation normally occurs from the ground state (S_0) of the fluorophore to the first electronically excited state (S_1). With enough energy higher excited states can be reached as well. Each electronic excitation state is divided into several vibrational states which all can be reached by light absorption. After excitation the fluorophore normally quickly returns emission-free to the lowest excited state with the lowest vibrational energy (S_1, v_0) through interaction with its surroundings. From there the transition back to the ground state occurs under emission of light (fluorescence). Sometimes the electron instead undergoes spin inversion dropping from an energetically higher singlet state to a triplet state, this process is called intersystem crossing. Return to the ground state occurs also under light emission but with reduced probability (phosphorescence). The orientation of the electron spin is marked with arrows, on the sides of the diagram.

Fluorescence can be measured either „steady-state“, with continuous excitation, or “time-resolved”, detecting the fluorescence decay after an excitation pulse to gain additional information about the fluorophores lifetime. All experiments in this work were performed with a steady-state fluorescence spectrometer (see fig. 1.6).

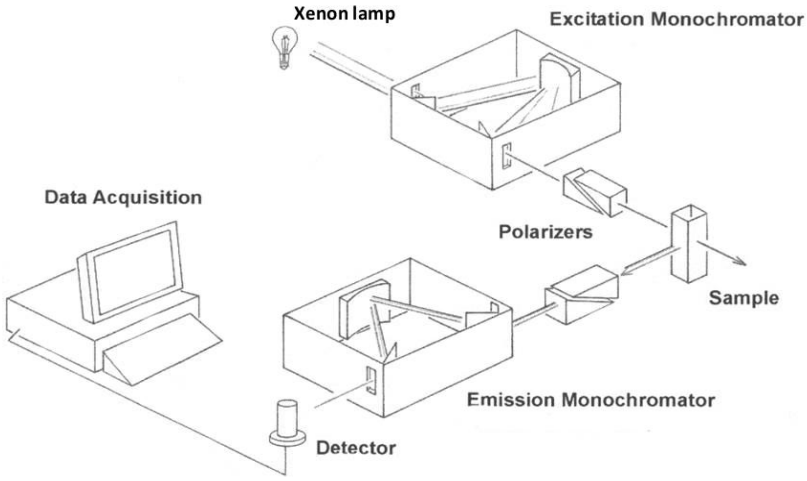

(Graphic adapted from the Varian Carry Eclipse Handbook)

Figure 1.6: Diagram of a steady-state fluorescence spectrometer: The sample is excited with a xenon lamp. The excitation wavelength is selected with a motorized monochromator which has been fitted with additional filters to minimize stray light. For anisotropy measurements hand-driven polarizers could be inserted into the light path. The emission is detected by a photomultiplier at a 90° angle to avoid detection of transmitted light.

To study proteins, the intrinsic fluorescence of their aromatic amino acids (phenylalanine, tyrosine and tryptophan) can be utilized. Of the three, tryptophan has the highest extinction coefficient and can be selectively excited between 295 – 305 nm. The emission maximum is near 350 nm in water and shifts towards shorter wavelength in a more apolar environment. Since the tryptophan fluorescence is highly sensitive to the local environment even small changes, caused by conformational change, protein interaction or substrate binding, can cause a shift of the peak maximum and/or changes in the fluorescence intensity.

The reduction of fluorescence intensity is called quenching. Tryptophan fluorescence can be statically quenched by electron transfer to nearby electron acceptors such as protonated carboxyl groups, disulfide or amide bonds. Förster resonance electron transfer to other aromatic amino acids can also reduce the observed fluorescence intensity. Bet3 has only one tryptophan (W96), which is ideal for quenching experiments because there is no overlap of different tryptophan spectra. Due to the sensitivity of tryptophan fluorescence, fluorescence quenching experiments can be used to study Bet3 substrate and membrane binding.

1.6 Fluorescence anisotropy

Anisotropy is defined as the directional dependence of a given material property. If a stationary fluorophore is excited with polarized light the emitted light is polarized as well. To determine the fluorescence anisotropy a sample is excited with vertical polarized light and the emission is then detected with polarization filters parallel and horizontal to the excitation polarization plane. The anisotropy (r) is given through the ratio of the intensity of vertical polarized emission to total emission:

$$r = \frac{I_{\parallel} - I_{\perp}}{I_{\parallel} + 2I_{\perp}}$$

$I_{\parallel}$: intensity of emission parallel, $I_{\perp}$: Intensity of emission horizontal to the excitation polarization plane.

If a fluorophore in solution is excited, the molecules will rotate in the span of the fluorescence lifetime, changing the orientation of the transition moments and thus the polarization plane of the emitted light. Hence the measurement of fluorescence anisotropy will yield information about the rotational speed of a molecule from which, under consideration of the solvent viscosity, information about molecule size and shape can be deduced. The value of “steady state” anisotropies can range between 0.4 and -0.2. The detailed deduction of the mathematical description of fluorescence anisotropy can be found in the appendix (chapter 9.2).

To gain information about the rotational correlation time, it has to be on the same timescale as the fluorescence lifetime. If the rotational speed greatly exceeds the lifetime, the sample will be disordered again at the point of emission and r will near zero, in the opposite case the molecules will have not rotated yet and r will near one. The rotational speed of proteins in solution, as well as of fluorophores in lipid layers is on the same time scale as the lifetime of many fluorophores, so that anisotropy lends itself well for the investigation of protein interaction or membrane fluidity.

To study Bet3 membrane binding the interaction with liposomes which function as membrane model is investigated. Because the apparent mass of Bet3 is greatly increased upon binding to the much larger liposomes, anisotropy measurements of the intrinsic tryptophan fluorescence can be employed to study Bet3 membrane binding.

1.7 Objectives

The TRAPP complex plays a vital role in protein trafficking through the cell by acting as a GEF for Rab GTPases and as a tether initiating the location of vesicular carriers to their destined organelle. Bet3 is a core subunit of the TRAPP complex and mediates membrane binding. Furthermore, Bet3 exhibits an unusual auto-palmitoylation activity.

The first goal of this work was to investigate the mechanism of Bet3 membrane binding. Three possible mechanisms for membrane binding were investigated: insertion of the covalently bound palmitate into the membrane, insertion of a fatty acid of the lipid bilayer into the hydrophobic tunnel of Bet3 and electrostatic interaction between a positively charged patch on the protein surface with the negatively charged hydrophilic heads of membrane lipids. For this purpose, the interaction of purified Bet3 (wild-type and mutants) with artificial model membranes of varied composition was determined by liposome flotation assays and fluorescence anisotropy.

The second goal was to further elucidate the auto-catalytic palmitoylation mechanism, in particular the substrate binding site. It had been shown that Bet3 is acylated with different acyl-CoAs, so one aim was to quantify the substrate binding properties of Bet3 in regard to acyl-CoAs of different length and shape. In addition, this works aimed at validating the hypothesis that the substrate binding site is inside the hydrophobic tunnel of Bet3. For this purpose, fluorescence quenching experiments with purified Bet3 (wild-type and mutants) and several acyl-CoAs and palmitoylation inhibitors were carried out.

2 Materials

2.1 Chemicals

Table 2.1: List of chemicals and manufacturers

Chemicals	Abbreviation	Manufacturer
[^{3}H]-Pal-CoA		Institute stock
1,4-Dithio-D,L-threitol	DTT	Roth
2-(N-morpholino)ethanesulfonic acid	MES	Serva
3-[(3-cholamidopropyl)dimethylammonio] -1-propanesulfonate	CHAPS	Roth
AccuTaq LA DNA-polymerase		Sigma
Acetic acid	AcOH	Merck
Acrylamide		Roth
Agar		Invitrogen
Agarose		Invitrogen
Ammonium persulfate	APS	Merck
Ampicillin	Amp	Roth
Bovine serum albumine	BSA	Sigma
Bromopalmitate	Br-Pal	ACROS ORGANICS
Bromophenol blue		Merck
Calcium chloride dihydrate	$CaCl_2 \cdot 2\ H_20$	Roth
Calf-intestinal phosphatase	CIP	NEB
Chloroform		Merck
Cholesterol	Chol	Sigma
Coenzyme A	CoA	Sigma
ColorPlus Prestained Protein Marker		NEB
Coomassie Brilliant Blue R 250	CBB R 250	Sigma
Disodium phosphate	Na_2HPO_4	Roth
DNA-Marker SmartLadder		Eurogentec
DNase I		Roche
dNTP mix		Stratagene
Ethanol	EtOH	Roth

Chemicals	Abbreviation	Manufacturer
Ethidiumbromide		Roth
Ethylenediaminetetraacetic acid	EDTA	AppliChem
Ethylene glycol-bis(β-aminoethyl ether)-N,N,N',N'-tetraacetic acid)	EGTA	Sigma
Fetal calf serum	FCS	Perbio
Ficoll 400		Sigma
Formaldehyde		Sigma
Glutathion, reduced		Sigma
Glycerol		Merck
Glycine		Roth
Hydrochloric acid	HCl	Roth
Isopropanol		Roth
Isopropyl β-D-1-thiogalactopyranoside	IPTG	Roth
Magnesium chloride hexahydrate	$MgCl \cdot 6\ H_20$	Serva
β-Mercaptoethanol		Roth
Methanol	MeOH	Roth
Milk powder		AppliChem
N-(7-nitro-2-3,1-benzooxadiazol-4-yl)dioleyl- phosphatidylcholine	NBD-PC	Sigma
N,N,N',N'-tetramethylendiamine	TEMED	Sigma
Nycodenz		Sigma
Phenylmethylsulfonyl fluoride	PMSF	AppliChem
Phosphatidylcholine	PC	Sigma
Phosphatidylethanolamine	PE	Sigma
Phosphatidylinositol	PI	Sigma
Phosphatidylserine	PS	Sigma
Potassium chloride	KCl	Roth
Potassium dihydrogenphosphate	KH_2PO_4	Roth
PreScission Protease		GE Healthcare
Restriction enzymes and buffers		NEB
Salicylate		Sigma
Sephardex-50-F		Pharmacia
Silver nitrate	$AgNO_3$	Sigma
Sodium carbonate	Na_2CO_3	Sigma
Sodium chloride	NaCl	Roth

Chemicals	Abbreviation	Manufacturer
Sodium cholate		Sigma
Sodium dodecyl sulfate	SDS	Biomol
Sodium thiosulfate	$Na_2S_2O_3$	Merck
T4-DNA-Ligase		NEB
Thrombin		Sigma
Trichloroacetic acid	TCA	Roth
Tris(hydroxymethyl)aminomethane	TRIS	Roth
Triton X-100		Serva
Tween 20		Sigma
YT Medium		Invitrogen

2.2 Kits and other materials

Table 2.2: List of used kits and other materials

Kit	Manufacturer
Invisorb Fragment CleanUp Kit	Invitek
Invisorb Plasmid Mini Two Kit	Invitek
PureYield Maxi Prep	Promega
DC Protein Assay Kit	BioRad
ECL plus Western Blotting Detection System	GE Healthcare
PVDF (Polyvinylidenfluoride) membrane	GE Healthcare
CL-XPosure film (for Western blot)	Perbio
Kodak Biomax XAR film (for fluorography)	Kodak
GSTrap FF column, 5 mL	GE Healthcare
HiTrap Benzamidin Column, 1 mL	GE Healthcare

2.3 Antibodies

Table 2.3: List of used antibodies

Antibody	Manufacturer
Mouse Anti-GST	Sigma
Anti-Mouse	Sigma

2.4 Laboratory equipment

Table 2.4: List of used laboratory apparatus, basic laboratory equipment is not listed.

Laboratory apparatus	Manufacturer
ÄKTA prime™ plus	GE Healthcare
Ultracentrifuge L7-65	Beckman Coulter
Ultracentrifuge TL-100	Beckman Coulter
Sonicator XL-2000	Misonix
Ultrasonic bath Branson 1210	Branson Ultraschall
Spectrometer Ultrospec® 500/1100 pro	Amersham Biosciences
NanoDrop 1000 spectrophotometer	PeqLab
Mircroplate reader	Tecan
Fluorescence spectrometer Cary Eclipse	Varian
CD spectrometer J720	Jasco
Western blot chamber	PeqLab
Chemiluminescence detection system Fusion SL	PepLab
Mini-Extruder (with polycarbonate filterø 100 nm)	Avanti Polar Lipids
Thermocyler mastercycler gradient	Eppendorf
Amicon Ultra Concentrators	Millipore

2.5 Buffers and solutions

Table 2.5: General buffers

Buffers	Composition	Concentration
PBS	NaCl	137 mM
	KCl	2.7 mM
	Na_2HPO_4	6.5 mM
	KH_2PO_4	1.5 mM
TRIS buffer	TRIS	5 mM
	NaCl	100 mM
	pH 7.4	

Table 2.6: Buffers for agarose gel electrophoresis

Buffers	Composition	Concentration
50x TAE buffer	TRIS	2 M
	EDTA	50 mM
	AcOH	1 M
	pH 8.0	
Gel buffer	TAE buffer with	
	ethidiumbromide	0.001 % (v/v)
5x DNA application buffer	TRIS-Borat	450 mM
	EDTA	5 mM
	bromophenol blue	0.01 % (w/v)
	Ficoll 400	20 % (w/v)
	pH 8.0	

Table 2.7: Buffers for Bet3 preparation

Buffers	Composition	Concentration
PBS buffer	see table 2.5	
GST elution buffer	TRIS	50 mM
	reduced glutathione	10 mM
	pH 8.0	
Thrombin binding buffer	TRIS	50 mM
	NaCl	1 M
	pH 7.4	
Thrombin elution buffer	HCl	10 mM
	NaCl	500 mM
	pH 3.0	
PreScission cleavage buffer	TRIS-HCl	50 mM
	NaCl	150 mM
	EDTA	1 mM
	DTT	1 mM
	pH 7.0	

Table 2.8: Buffers for SDS-PAGE [27]

Buffers	Composition	Concentration
Sample buffer	Tris-HCl, pH 6.8	62.5 mM
	SDS	2 % (w/v)
	glycerol	10 % (v/v)
	bromophenol blue	0.1 % (w/v)
Reducing sample buffer	sample buffer plus β-mercaptoethanol	5 % (v/v)
Electrophoresis buffer	Tris-HCl,pH 8.3	25 mM
	Glycin	192 mM
	SDS	0.1 % (w/v)
Stacking gel buffer	Tris-HCl, pH 6.8	125 mM
	SDS	0.4 % (w/v)
Separating gel buffer	Tris-HCl, pH 8.8	375 mM
	SDS	0.4 % (w/v)

Table 2.9: Composition of SDS gels

	%-acrylamide		
	stacking gel	separating gel	
Composition	5 %	12 %	15 %
Buffer	625 µL	1.875 mL	1.875 mL
Acrylamide/bisacrylamide (37.5:1; 30 % solution)	415 µL	3.0 mL	3.75 mL
APS 10 % (w/v)	20 µL	40 µL	40 µL
TEMED	3.5 µL	7 µL	7 µL
Destilled water	1.435 mL	2.575 mL	1.825 mL

Table 2.10: Solutions for CBB staining

Solutions	Composition	Concentration
Staining solution	EtOH	50 % (v/v)
	AcOH	10 % (v/v)
	CBB R250	0.1 % (w/v)
Destaining solution	EtOH	10 % (v/v)
	AcOH	10 % (v/v)

Table 2.11: Solutions for silver staining

Solution	Composition	Concentration
Fixer	EtOH	40 % (v/v)
	AcOH	10 % (v/v)
	formaldehyde (37 %)	0.5 % (v/v)
Silver staining solution	$AgNO_3$	0.16 % (w/v)
	formaldehyde (37 %)	0.075 % (v/v)
Developer	Na_2CO_3	5 % (w/v)
	$Na_2S_2O_3$	0.025% (w/v)
	formaldehyde (37 %)	0.04 % (v/v)

Table 2.12: Buffers for Western blots [28]

Buffers	Composition	Concentration
Blot buffer	TRIS-HCl, pH 7.5	25 mM
	glycine	192 mM
	SDS	0.5 % (w/v)
	methanol	20 % (v/v)
Blocking buffer	PBS with	
	Tween 20	0.1 % (v/v)
	milk powder	5 % (w/v)

Table 2.13: Buffer for the SUV assay

Buffers	Composition	Concentration
Assay buffer	TRIS	50 mM
	NaCl	100 mM
	EGTA	100 nM
	pH 7.5	
Micelle buffer	assay buffer with	
	CHAPS	18 mM

Table 2.14: Buffers for the palmitoylation assay

Solution	Composition	Concentration
^{3}H-Palmitate buffer	Tris-HCl	20 mM
	NaCl	120 mM
	Triton X-100	0.05 %
	pH 7.4	
pH 6.5	MES	20 mM
	NaCl	120 mM
pH 7.5	TRIS	20 mM
	NaCl	120 mM
pH 8.5	TRIS	20 mM
	NaCl	120 mM

2.6 Oligonucleotides

Table 2.15: Used oligonucleotides (synthesized by Bio TeZ Berlin Buch)

Oligonucleotide	Sequence (5' → 3')
Bet3 *Bam*HI fwd	TCC GCG TGG ATC CTC GAG GC G
Bet3 *Not*I rev	C ACG ATG CGG CCG CTT CCT CT
A138V fwd	TTG CGG GGA GTT TTG GAG ATG GTC
A138V rev	GAC CAT CTC CAA AAC TCC CCG CAA

2.7 Bacteria strains and vectors

Table 2.16: Used bacteria strains

Strain	Genotype	Reference
BL21(DE3)	F^- d*cm ompT hsdS*(r_B^- m_B^-) *gal λ*(DE3)	Agilent Manual http://www.agilent.com/cs/library/usermanuals/Public/200133.pdf
XL-1 blue	*rec*A1 *end*A1 *gyr*A96 *thi*-1 *hsd*R17 *sup*E44 *rel*A1 *lac* [F´ *pro*AB *lac*IqZΔM15 Tn10 Tet^r]	http://www.genomics.agilent.com/de/Competent-Cells-Routine-Cloning/General-Cloning/?cid=AG-PT-120&tabId=AG-PR-1058&searchText=200249

Table 2.17: Used vectors, vector maps can be found in the appendix

Vector	Reference
pGex-4T1 pGex-6P1	GE Healthcare Handbook http://www.gelifesciences.com/file_source/GELS/Service%20and%20Support/Documents%20and%20Downloads/Handbooks/pdfs/GST_gene_fusion_system_handbook.pdf

3 Methods

3.1 Microbiological methods

3.1.1 Protein expression

For protein preparations three times 450 mL YT medium with ampicillin (final concentration100 µg/mL) in 1 L Erlenmeyer flasks with baffles were inoculated with *E.coli* and incubated at 37 °C. At an OD_{600} of 0.6 protein expression was induced with IPTG (final concentration 100 nM). Upon entering the stationary growth phase (determined by measuring the OD) the cells were harvested by centrifugation (4 °C, 10 min, 8000 rpm / 10000*g, Avanti J25 High-performance centrifuge, Rotor JLA-16.250). The bacterial sediment was washed with 50 mL PBS buffer, weighed, quick-frozen in $N_{2\ (fl.)}$ and stored at –80 °C.

3.1.2 Chemically competent cultures

To produce chemically competent cells for heat shock transformation 3 mL YT medium were inoculated with 1 µL of XL-1-blue or with BL21(DE3) stock and incubated over night at 37° C. Twice 100 mL YT medium were inoculated with 1 mL overnight culture and incubated at 37 °C until reaching an OD_{600} of 0.5. The cells were then incubated on ice for 30 min and finally harvested by centrifugation (4 °C, 10 min, 8000 rpm / 10000*g, Avanti J25 High-performance centrifuge, Rotor JLA-16.250). The pellet was transferred in a 50 mL Falcon tube, washed with 25 ml cold $CaCl_2$ (50 mM), resuspended, incubated on ice for another 30 min and centrifuged (10 min, 4 °C, 5000 rpm / 4500*g, Eppendorf Centrifuge 5804 R). Then the cells were resuspended in 5 ml 50 mM $CaCl_2$ and 1.25 mL glycerol (80 %) was added. The competent cultures were quick-frozen in 650 µL aliquots and stored at –80 °C.

3.1.3 Heat shock transformation

30 – 200 ng DNA were added to 300 µL ice cold, chemically competent cells and incubated on ice for 30 min, followed by a heat shock of 45 sec at 42 °C and another 2 min incubation on ice. 600 µL YT medium were added and the cells were incubated for 1 h at 37 °C to allow for the formation of antibiotic resistance. Afterwards the transformed cells were plated on YT agar plates (with ampicillin 100 µg/mL) and incubated over night at 37° C. Following the introduction of point mutations XL-1-blue cells were transformed with the freshly ligated DNA. For protein expression the BL21(DE3) strain was transformed with plasmid DNA extracted from those XL-1-blue cells.

3.2 Molecular biological methods

3.2.1 Introduction of point mutations by site-directed mutagenesis

Point mutations were introduced by site-directed mutagenesis based on overlap extension (AB-PCR) [29, 30] (see fig. 3.1).

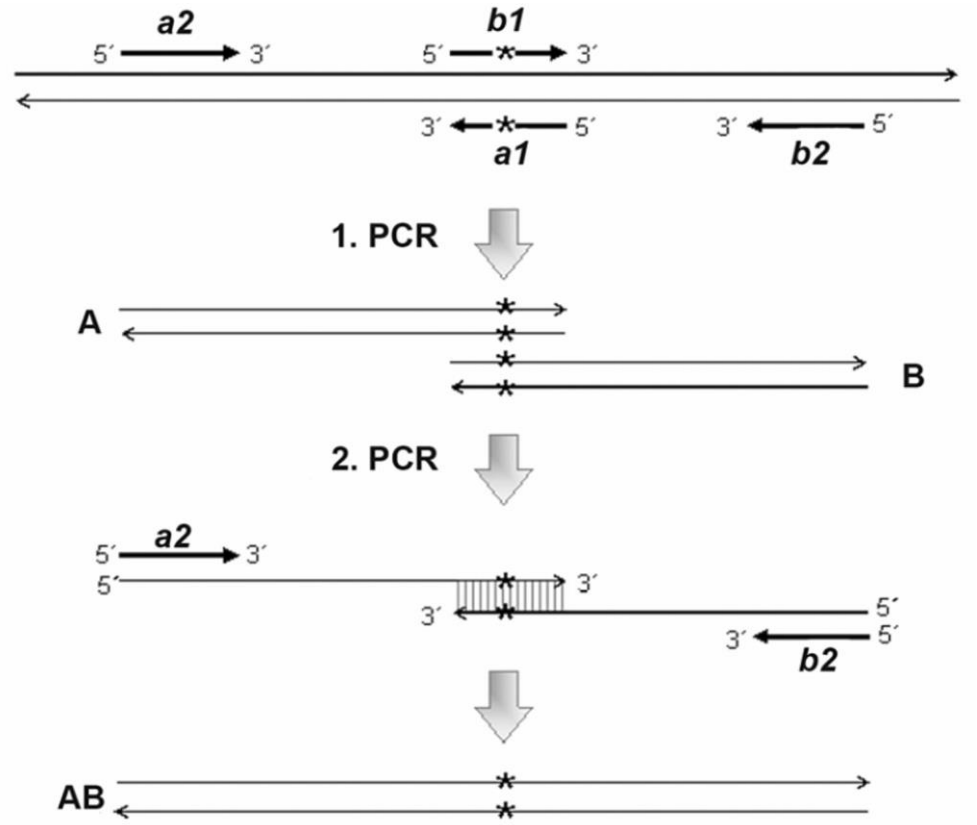

(Veit et al., Analysis of S-acylation of proteins. Methods Mol Biol, 2008)

Figure 3.1: Schematic diagram of the AB-PCR [30]: The outer primers a2 and b2 code for the restrictions sites, the inner, complimentary primers a1 and b1 contain in the middle the new point mutation. In the first PCR round the template is amplified in two batches with either the A or B primer, resulting in short DNA fragments which are complimentary to one another in the area of the point mutation. These fragments serve as templates in the second PCR. With the outer primers used, the resulting product contains the point mutation as well as the restriction sites needed for ligation into the vector.

For the AB-PCR four primers are required, two outer primers coding for a restriction site (*a2, b2*) and two inner, complimentary primers containing the new point mutation (*a1, b1*). The first round of PCR is carried out with two distinct reaction batches amplifying the template with either A (*a1, a2*) or B (*b1, b2*) primers. This way short DNA fragments (A and B) are produced which are complimentary to one another in the area of the point mutation and are used as templates in a second round of PCR. By using the outer primers in the second PCR (*a2, b2*) a DNA fragment (AB) containing two restriction sites and the desired point mutation is produced. The original DNA fragment in the vector can now be replaced with the new AB fragment.

Both PCRs were performed with an Eppendorf Master cycler in 50 µL samples. In the first PCR the vector pGex-4T1 Bet3 A82V was used as template. In sample A the forward primer contained the mutation A138V and the reverse primer the restriction site *Not*I, in sample B the forward primer contained the restriction site *Bam*HI and the reverse primer the mutation. Each sample contained the following mixture and the PCR was performed according to the program below.

per sample	
buffer	5 µL
ddH_2O	38 µL
template	2 µL
$MgCl_2$	1.5 µL
dNTPs	1 µL
polymerase Acu-Taq	0.5 µL
primer fwd	1 µL
primer rev	1 µL

PCR program 1		
94 °C	1’	
94 °C	30”	⎫
55-57 °C	30”	⎬ 30x
68 °C	30”	⎭
68 °C	10’	
10 °C	∞	

The products of the first PCR were purified by agarose gel electrophoresis and served as templates (A, B) in the second PCR The second PCR contained the following mixture and the PCR was performed according to the program below.

per sample	
ddH_2O	39-45 µL
buffer	5 µL
$MgCl_2$	1.5 µL
dNTPs	1 µL
polymerase Acu-Taq	0.5 µL
primer *Bam*HI fwd	1 µL
primer *Not*I rev	1 µL
fragment A	2-5 µL
fragment B	2-5 µL

PCR program 2		
94 °C	1’	
94 °C	30”	⎫
55-57 °C	30”	⎬ 20x
68 °C	40”	⎭
68 °C	10’	
10 °C	∞	

The PCR product was again purified by agarose gel electrophoresis and digested with the restriction enzymes *Not*I and *Bam*HI in preparation of the ligation step.

3.2.2 Ligation

Vector and insert were both digested with *Not*I and *Bam*HI for 2 h at 37 °C to prepare the ligation sites.

Insert (PCR product)	Vector (plasmid pGex-GST-Bet3)
20 µl AB fragment	5.5 µl vector
3 µl buffer #3	2 µl buffer #3
3 µl BSA (10 mg/mL)	2 µl BSA (10 mg/mL)
1 µl *Not*I	1 µl *Not*I
1 µl *Bam*HI	1 µl *Bam*HI
2 µl H_2O	9.5 µl H_2O

30 min before the end of incubation the linearized vector is dephosphorylized by addition of 1 U calf-intestinal phosphatase to avoid re-ligation. The digested fragments were purified by agarose gel electrophoresis. Insert and linearized vector were mixed and incubated for 1 h at room temperature with T4 ligase.

per ligation batch
16 µl digested insert
1 µl digested vector
2 µl ligase buffer
1 µl T4 ligase

Afterwards the newly formed plasmid was used for heat shock transformation of competent XL-1-blue cells.

3.2.3 Agarose gel electrophoresis

For the electrophoresis gels made of 0.8 % (w/v) agarose in TAE buffer with 0.001 % (v/v) ethidiumbromide were used. The DNA fragments were separated for 20 - 40 min at 100 mA. The desired plasmid fragments were detected with UV light (302 nM wavelength) through comparison with a molecular weight marker (SmartLadder, Eurogentec), cut from the gel and extracted with the Invisorb Fragment CleanUp Kit according to manufacturer's instructions. The purified DNA was eluted with 20 µL ddH_2O. (Buffers see table 2.6.)

3.2.4 Analytical plasmid preparation

To obtain plasmid for DNA sequencing single bacteria colonies (Xl-1 blue strain transformed with plasmids obtained by PCR mutagenesis) were picked from agar plates and incubated at 37 °C overnight in 3 mL YT medium with ampicillin (final concentration 100 µg/mL). The next day the cells were harvested and the plasmid DNA purified with an Invisorb Plasmid Mini Two Kit according to manufacturer's instructions and eluted with 50 µL 50 °C warm ddH_2O. DNA concentration was determined with a NanoDrop spectrophotometer.

The plasmid was controlled by an analytical restriction digest. Each 30 µl sample contained 5 µl plasmid, 3 µl buffer #3, 3 µl BSA (10 mg/mL), 1 µl *Not*I and 1 µl *Bam*HI and was incubated for 2 h at 37 °C. The digest was analyzed by agarose gel electrophoresis. Sequencing of new mutants was performed by GATC Biotech AG using the sequencing primer pGex5-FP (AACGTATTGAAGCTATCCC).

3.2.5 Preparative plasmid preparation

For protein expression BL21(DE3) cells were transformed with at least 100 ng plasmid DNA. To obtain sufficient quantities of plasmid XL1-blue cells containing the plasmid were harvested from a 200 mL overnight culture in YT medium with ampicillin (final concentration 100 µg/mL) and the plasmid was purified with the PureYield Maxi Prep system according to manufacturer's instructions. The purified DNA was eluted with 1 ml ddH_2O and the DNA concentration was determined with a NanoDrop spectrophotometer.

3.2.6 Protein expression test

To check the successful expression of a new protein mutant the relevant plasmid was introduced in to chemically competent BL21(DE3) cells by heat shock transformation. The transformed cells were plated on YT agar plates (with ampicillin 100 µg/mL) and overnight cultures from single bacteria colonies were picked the next day. From each of these overnight cultures two times 3 mL YT medium with ampicillin (final concentration 100 µg/mL) was inoculated and incubated for 2 h at 37 °C. One of the two 3 mL cultures was then induced with IPTG (final concentration 100 nM) and both cultures were incubated for another 2 h. Cells were harvested by centrifugation from 50 µL of each culture (induced and non-induced). The pellet was resuspended in 20 µL SDS sample buffer and heated for 5 min to 95 °C. GST-Bet3 expression was verified by SDS-PAGE followed by a Western blot with mouse anti-GST antibody.

3.3 Protein methods

3.3.1 Protein assays

Lowry protein assay

The protein concentration was determined using a DC Protein Assay Kit (BioRad) according to manufacturer's instructions. The absorption at 750 nm was measured with a Tecan Miroplate Reader in conjunction with the analysis program „easy Win curve fitting" (Tecan).

Concentration determination through absorbance at 280 nm

The protein concentration was determined through the absorption at 280 nm following the Lambert-Beer law and using a NanoDrop spectrophotometer. The extinction coefficient of Bet3 is 11'500 cm^{-1} M^{-1} (as calculated from the DNA sequence), the coefficient of GST-Bet3 is 54'500 cm^{-1} M^{-1}. The molecular weight of Bet3 was calculated to 22.3 kDa and for GST-Bet3 to 50.1 kDa.

3.3.2 Protein preparation

Preparation of GST-Bet3

3 – 5 g *E.coli* cells were resuspended in 30 mL ice cold PBS buffer (with 1 mM DTT, 1 mM PMSF and DNase) and lyzed by sonication with five 10 sec pulses (15 – 20 Watt). Cell debris was sedimented through centrifugation (23000 rpm / 413550*g, Ti 45, 40 min, 4 °C).

The supernatant was added to a 5 mL GSTrap FF Column (flow rate 0.5 ml/min). After washing with PBS buffer the bound protein was eluted with GST elution buffer (0,5 ml/min, 2 ml fractions).

The fractions containing protein were pooled. Buffer exchange to PBS and concentration were achieved by ultrafiltration (Amicon Ultra concentrator, 10 kDa MWCO, 4 °C, 5000 rpm / 4500*g, Eppendorf Centrifuge 5804 R). Protein purity was verified by SDS-PAGE. The protein was divided into aliquots, quick-frozen in $N_{2\,(fl.)}$ and stored at –80 °C. (Buffers see table 2.7.)

Preparation of untagged Bet3 through thrombin cleavage

Since the GST tag interfered with some assays, the GST could be removed in those cases in the course of protein preparation. The vector pGex-4T-1 codes for a thrombin cleavage site between GST and Bet3.

Protein preparation followed the GST-Bet3 preparation protocol up to binding of GST-Bet3 on the GSTrap FF column. After washing with PBS buffer, 100 U thrombin (in PBS plus 850 mM NaCl) were applied and the protein was incubated on the column over night at room temperature. Then the protein was eluted over a 1 mL HiTrap Benzamidin column with thrombin binding buffer (0.5 mL/min, 2 mL fractions). The fractions containing protein were pooled. Buffer exchange to PBS and concentration were achieved by ultra-filtration (Amicon Ultra concentrator, 10 kDa MWCO, 4 °C, 5000 rpm / 4500*g, Eppendorf Centrifuge 5804 R). Protein purity was verified by SDS-PAGE. The protein was divided into aliquots, quick-frozen in $N_{2\ (fl.)}$ and stored at –80 °C. The GSTrap FF column was regenerated with GST elution buffer, the HiTrap Benzamidin column with thrombin elution buffer. (Buffers see table 2.7.)

Preparation of untagged Bet3 through PreScission protease cleavage

Because Bet3 KKEE was encoded in a pGex-6P-1 vector instead of a pGex-4T-1 vector Bet3 KKEE was prepared using PreScission protease cleavage. pGex-6P-1 codes for a PreScission protease cleavage site instead of a thrombin cleavage site. Protein preparation followed once again the GST-Bet3 preparation protocol up to binding of GST-Bet3 on the GSTrap FF column. After washing with PreScission cleavage buffer, 800 U PreScission protease were applied and the protein was incubated on the column over night at 4 °C. Then the protein was eluted with PBS buffer (0.5 mL/min, 2 mL fractions).

The fractions containing protein were pooled and concentrated by ultra-filtration (Amicon Ultra concentrator, 10 kDa MWCO, 4 °C, 5000 rpm / 4500*g, Eppendorf Centrifuge 5804 R). Protein purity was verified by SDS-PAGE. The protein was divided into aliquots, quick-frozen in $N_{2\ (fl.)}$ and stored at –80 °C. The GSTrap FF column was regenerated with GST elution buffer. (Buffers see table 2.7)

3.3.3 Other protein methods

SDS-PAGE

For SDS-PAGE discontinuous SDS gels [27], with 5 % stacking gel and 12-15 % separating gel were used (see table 2.9). If necessary, the protein was concentrated by TCA precipitation beforehand. SDS sample buffer was added to the protein and the sample was denaturated by heating to 95 °C. Electrophoresis was performed with a constant voltage of 90 V until the protein entered the separating gel and continued with 180 V until the dye front reached the end of the gel. After electrophoresis gels were stained with Coomassie and/or silver staining. (Buffers see table 2.8.)

Coomassie staining

After electrophoresis SDS gels were incubated in CBB staining solution for 30 min and then de-stained in de-staining solution until the background was clear again and the protein bands clearly visible. To speed up dye removal the de-staining solution was exchanged 1-2 times. The de-stained gels were scanned or documented with the chemiluminescence detection system Fusion SL (PeqLab) and dried for storage. The quantitative analysis was performed with the Bio1 software (PeqLab).
(Solutions see table 2.10.)

Silver staining

After SDS-PAGE the gels were incubated for 1 h at room temperature in fixer and then washed three times in EtOH/H_2O (1:1) for 30 min. Afterwards the protein in the gels was reduced by 1 min incubation with 0.02 % $Na_2S_2O_3$•$3.5H_2O$ (w/v) and washed three times in water for 20 sec. Then the gels were incubated in silver staining solution for 30 min and once again washed 20 sec in water twice. Then the gels were incubated in developer until the silver staining became visible. The reaction was stopped by 1 min bathing in 1 % (v/v) glycerol. After washing in water the gels were incubated for 10 min in 10 % (v/v) ethanol with 2 % (v/v) glycerol and dried for storage.
(Solutions see table 2.11.)

TCA precipitation

To achieve the protein concentrations necessary for SDS-PAGE the protein could be concentrated by TCA precipitation.

An equal volume trichloro acetic acid (TCA, 20 % (w/v)) was added to the protein solution and incubated on ice for 20 min. The protein was sedimented by centrifugation (4 °C, 30 min, 12000 rpm/15000*g, Eppendorf Centrifuge 5417 R) and the supernatant discarded. The pellet was washed twice with ice cold 100 % ethanol and centrifuged once again (4 °C, 5 min, 12000 rpm/15000*g, Eppendorf Centrifuge 5417 R). Then the supernatant was completely removed and the protein resuspended in SDS sample buffer. (Buffer see table 2.8.)

Western blot

For the detection with antibodies the proteins were electrophoretically transferred to a PVDF (polyvinylidene fluoride) membrane after SDS-PAGE. The transfer was performed with 110 mA per gel (6 × 8 cm) in a semi-dry blotting chamber for 70 min. Then the membrane was incubated in blocking buffer for 1 h and afterwards treated over night at room temperature with the first antibody (anti-GST 1:4‘000). After washing thrice for 10 min with blocking buffer, the membrane was incubated with the second antibody (anti-mouse 1:5‘000) for 1 h at room temperature. After washing once again the membrane was treated with the ECL plus Western Blotting Detection System according to manufacturer’s instructions. A CL-XPosure film was exposed with the membrane for 0.5 – 15 min, developed and scanned for documentation. (Buffers see table 2.12.)

3.4 Fluorescence spectroscopic methods

3.4.1 Fluorescence spectroscopic determination of Bet3 acyl-CoA binding

Binding of different acyl-CoAs to Bet3 wild-type and mutants was determined via the change in the intrinsic tryptophan fluorescence of Bet3 upon interaction with acyl-CoAs. All measurements were performed at room temperature using a Cary Eclipse fluorescence spectrophotometer (Varian) in a 100 µL quartz glass cuvette. The excitation wavelength was 295 nm. Emission was detected from 310 – 450 nm. Each emission spectrum was measured five times and an average spectrum calculated. The emission maximum was read at 344 nm.

Purified Bet3 was diluted in TRIS buffer to a final concentration of 10 µM. The emission spectrum was determined as described above. Then the acyl-CoA concentration was increased step by step by adding 1 µL stock solution (1-100 mM acyl-CoA in TRIS buffer) and the emission spectra and the intensity of the emission maximum were determined after each step.

The fluorescence intensity was normalized (F_0–F/F_0; F_0: fluorescence intensity without ligand, F: fluorescence intensity at any given acyl-CoA concentration) and plotted against the acyl-CoA concentration. Acyl-CoA binding to Bet3 can be described with:

$$Y = \frac{K_D + L + nP - \sqrt{(K_D + L + nP)^2 - (4LnP)}}{2nP/Y_{max}}$$

(K_D: apparent dissociation constant for acyl-CoA, L/P: ligand/protein concentration, n: number of ligand binding sites per protein and Y_{max}: maximal change in fluorescence intensity). The graphs were analyzed with the program Prism (GraphPad), the protein concentration was fixed to 10 µM. K_D, n and Y_{max} were free variables. The model is based on a bimolecular reaction with depletion of both reactants (see appendix chapter 9.3) [31].

3.4.2 SUV assay

To investigate membrane binding of Bet3 SUVs (small unilamellar vesicles) were used as a membrane model. SUVs are 25-100 nm in size and are better suited for detecting changes in fluorescence intensity than the larger LUVs (large unilamellar vesicles) because they cause less light scattering.

Preparation of SUV

The SUV were prepared with the following composition (in mol %): PC 50 %, PE 20 %, PI, PS and Cholesterol 10 %. The lipids were mixed in chloroform and the solvent was evaporated using a very weak nitrogen flow. By applying vacuum in an exsiccator over night the solvent was completely dried off.

The lipids were resuspended in 1 mL micelle buffer (final concentration 2 mM). This lipid solution was diluted with assay buffer to 1 µM, 10 µM, 100 µM, and 1 mM. These stock solutions were finally sonicated for 1 min on ice with a microtipsonicator to obtain homogenously sized SUVs.

Determining the Bet3 SUV interaction

Fluorescence spectra were measured in 100 µL assay buffer at room temperature using a Cary Eclipse fluorescence spectrophotometer (Varian) and a 100 µL cuvette. The excitation wavelength was 295 nm. Emission was detected from 290-450 nm.

First the fluorescence of the assay buffer was determined. It was subtracted as a baseline from all following spectra.

Since the detergent CHAPS in the buffer of the SUV stock solution fluoresces at the same wavelength as tryptophan, the intrinsic fluorescence of the SUV stock solutions was determined. The SUV concentration in the assay buffer was increased stepwise according to the pipetting scheme in table 3.18 and the fluorescence spectra recorded.

µL SUV stock solution with a concentration of				final lipid concentration	final CHAPS concentration
1µM	10µM	100µM	1mM		
1				10 nM	90 nM
2				30 nM	270 nM
	1			130 nM	1170 nM
	2			330 nM	2970 nM
		1		1330 nM	11970 nM
		2		3330 nM	29970 nM
			1	13330 nM	119970 nM
			2	33330 nM	299970 nM

Table 3.18: Pipetting scheme SUV assay.

In a second step the binding of Bet3 to SUVs was determined. Purified Bet3 was diluted with assay buffer to a final concentration of 100 nM. After recording the fluorescence spectrum of pure protein, the lipid concentration in the sample was once again increased stepwise (see table 3.18) and each time the fluorescence measured. (Buffers see table 2.13).

To calculate the change in fluorescence intensity with increasing lipid concentration, from each spectrum the according lipid-only spectrum was deducted so that the influence of the increasing CHAPS concentration could be excluded. The intensity at 340 nm of the net tryptophan fluorescence spectra was determined and plotted against the lipid concentration. K_D values were calculated with

$$y = \frac{Y_{max} \cdot x}{K_D + x}.$$

3.4.3 Anisotropy assay

Due to their lesser surface curvature LUVs are better membrane models than SUVs. To minimize the problems caused by increased light scattering the Bet3 LUV interaction was observed via the reduced rotational velocity of Bet3 upon binding to LUVs using anisotropy measurements. The LUVs were prepared using an extruder because this method allows for a more exact estimation of the final lipid concentration.

Liposome preparation with an extruder

A 2 mL glass vial with a conical bottom was washed with chloroform. Then the desired lipid mixture was dissolved in chloroform/methanol (9:1). While constantly rotating the glass vial slowly the solvent was evaporated using a very weak nitrogen flow. By applying vacuum in an exsiccator over night the solvent was completely dried off. The lipids were resuspended in PBS buffer (final concentration 1 mg/mL) and agitated for 30 min at room temperature until the lipid layers peeled away from the glass wall. If necessary, the vial was shortly vortexed to dissolve lipid layers remaining on the glass wall. The suspension was sonicated for 15 – 30 min in a 30 °C warm ultrasonic bath. Then the lipid suspension was passed 11-25 times through the extruder until the suspension had noticeably cleared (see fig. 3.2). The filtration process can cause a loss of up to 100-200 µl liquid and 10-30 % of lipids.

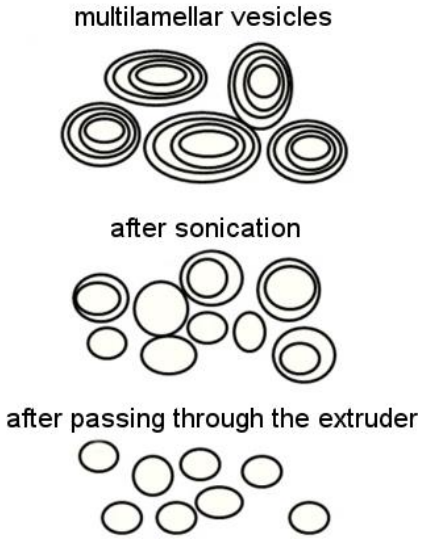

Figure 3.2: Schematic diagram of LUV

All fluorescence anisotropy measurements were performed at room temperature using a Cary Eclipse fluorescence spectrophotometer (Varian) with polarization filters in a 100 µL quartz glass cuvette. The excitation wavelength was 295 nm. Emission was detected at 338 nm.

Purified Bet3 was diluted with PBS buffer to a final concentration of 10 nM and the anisotropy of the intrinsic tryptophan fluorescence determined. The liposome concentration was increased in 20 µM steps by adding liposome stock solution and the fluorescence intensity measured for all four polarizer positions (see chapter 1.5) after each step. Each value was determined five times, averaged and the anisotropy calculated as follows:

$$r = \frac{I_{VV} - GI_{VH}}{I_{VV} + 2GI_{VH}}$$

The change in anisotropy was plotted against the lipid concentration.

To ascertain that the change in anisotropy was really due to protein liposome binding and not caused by binding interaction with single lipids the liposomes were destroyed with Triton X-100 (final concentration 0.1 % (v/v)) at the end of a measurement series and the anisotropy determined once more.

Estimation of the lipid concentration required for anisotropy measurements

To achieve sufficient signal intensity, the minimum protein concentration was 10 µM. On the other hand, to reliably observe a change in anisotropy a tenfold surplus of binding sites for each protein is required. Based on these prerequisites the required lipid amount was estimated as follows: The average diameter of a lipid is 0.7 nm, the diameter of the liposomes circa. 100 nm, therefore one liposome consists of about 100‘000 lipids. The diameter of Bet3 was estimated to be 5 nm. Assuming that the liposome surface covered by one Bet3 protein equals one fourth of the surface of Bet3, it can be concluded that approximately 100 lipids are required to bind one Bet3 protein. Following this conclusion, the liposome stock solution was prepared with a lipid concentration of 10 µM.

3.5 Other methods

3.5.1 Palmitoylation assay

[^{3}H]-Pal-CoA used for radioactive labeling had been synthesized according to [32]. In 100 µL buffer of desired pH GST-Bet3 (final concentration 4 µM) was mixed with 5 µL [^{3}H]-Pal-CoA (in ^{3}H-palmitate buffer, circa 1 µM/100000 cpm/µl) and DTT (final concentration 1 mM) and incubated for 20 min at 30 °C. 1 mL ice cold chloroform/methanol (1:2) was added to each batch and incubated on ice for further 10 min. The precipitated protein was sedimented by centrifugation (15 min, 14000*g, Eppendorf Centrifuge 5417 R), washed with ice cold methanol and dried. Then the protein was resuspended in 20 µL non-reducing SDS sample buffer and analyzed by SDS-PAGE. The gels were first stained with Coomassie staining, documented and completely de-stained afterwards. For fluorographic detection the gels were washed twice for 15 min in H_2O and incubated in 1 M salicylate for 30 min. After drying the gels were exposed to an X-ray photo film for at least two days. (Buffers see table 2.14).

3.5.2 Liposome flotation assay

LUV preparation through detergent removal

The desired lipid mixture was dissolved in chloroform in 2 mL glass vial. To facilitate detection of the liposomes 1 % NBD-PC was added to the mixture. Then the solvent was evaporated using a very weak nitrogen flow. By applying vacuum in an exsiccator over night the solvent was completely dried off. The lipids were resuspended in 1 mL PBS buffer with 5 % (w/v) cholate and applied to a 30 mL Sephardex-50-F column. The cholate was removed by gel filtration (flow rate 1 mL/min) and liposomes formed on the column (see fig. 3.3). The liposome containing fractions were detected using UV light and pooled.

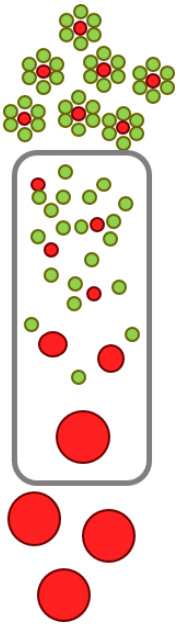

Figure 3.3: Schematic diagram of LUV formation through detergent removal by size exclusion gel chromatography. The lipids are fist mobilized by the smaller detergent molecules. The detergent is then retained on the column thus freeing the lipids again and liposomes form to reduce the free energy by decreasing the contact area of hydrophobic lipids with water.

Density gradient centrifugation

Purified Bet3 (final concentration 2-5 µM) was added to 200 µL liposome stock prepared by detergent removal and incubated for 15-30 min at room temperature. Then Nycodenz was added to a final concentration of 40 % (w/v). The liposome solution was pipetted in a centrifugation tube and layered with 400 µL 30 % Nycodenz (w/v in PBS) and 100 µL PBS buffer. During centrifugation (4 h, 4 °C, 23000 rpm/186000*g, SW 55 Ti) the liposome-bound protein floated upwards. After centrifugation the gradient was fractioned into 100 µL fractions top-downward. The protein in each fraction was concentrated by TCA precipitation and analyzed by SDS-PAGE followed by Coomassie and silver staining (see fig. 3.4).

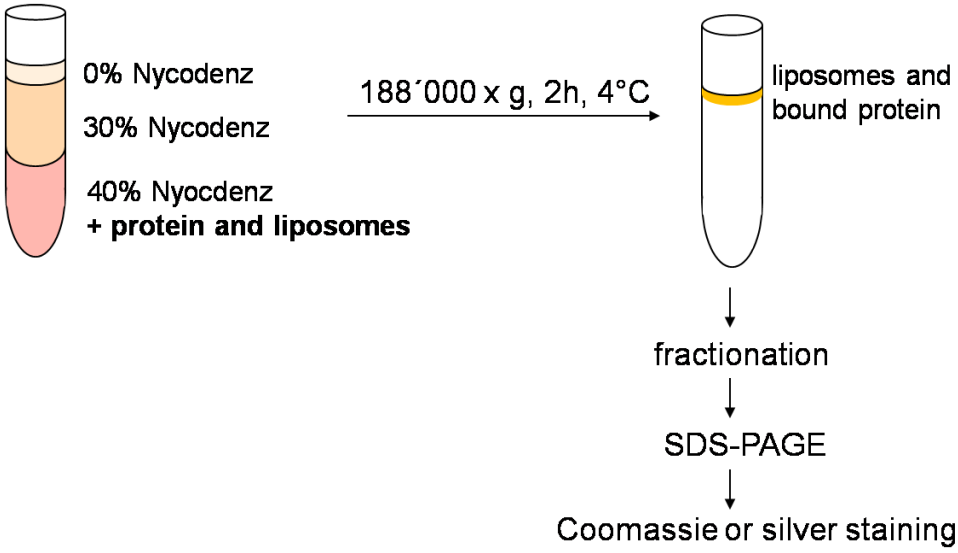

Figure 3.4: Schematic diagram of the liposome flotation assay. The protein is mixed with the liposomes and placed at the bottom of a density gradient. After centrifugation bound protein has floated with the liposomes to the top of the gradient

3.5.3 CD spectroscopy

For CD spectroscopy purified Bet3 was diluted to 0.16 mg/mL in PBS buffer. Measurements were performed with a Jasco J720 spectropolarimeter at 20 °C from 200 nm to 260 nm in a 0.2 cm path length cuvette.

.

4 Results

4.1 Preparation of Bet3

Since all experiments were conducted *in vitro* using purified protein, an exemplary preparation of GST-Bet3 wild-type and tag removal is presented in this chapter.

Purification of Bet3 was carried out by binding of GST-tagged protein to a GSTrap FF column and yielded high protein purity in all preparations. *E.coli* cells transfected with the protein expressing plasmid were grown in YT medium to an OD_{600} of 0.6 and induced with IPTG. Upon entering the stationary growth phase cells were harvested by centrifugation (see fig. 4.1 A).

To determine the required amount of thrombin for GST-Bet3 cleavage, 7 µg GST-Bet3 were incubated with 10 U, 1 U and 0.1 U thrombin for 4 h at room temperature and analyzed by SDS-PAGE. All three samples showed complete cleavage and no signs of degradation (see fig. 4.1 B). Since 0.1 U of thrombin were sufficient to cleave 7 µg protein and preparations of GST-Bet3 usually yielded about 5 mg protein, further preparations of untagged Bet3 were performed with 100 U thrombin.

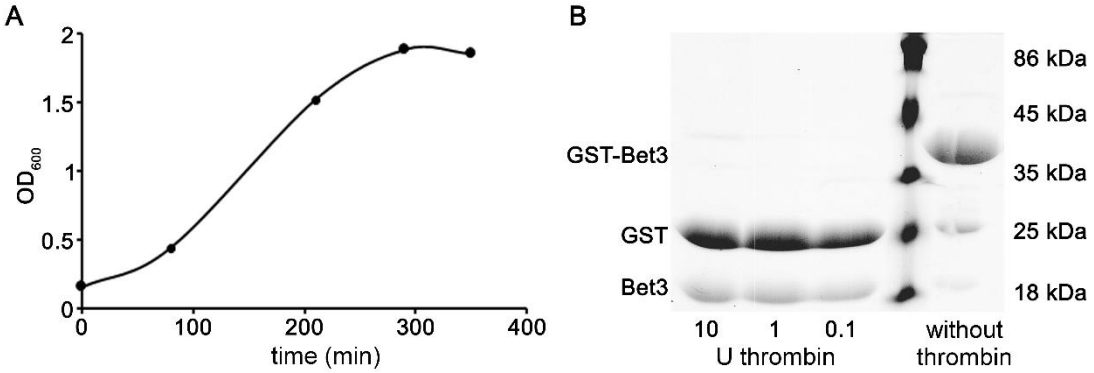

Figure 4.1: (A) Typical growth curve of *E. coli* BL21(DE3) with Bet3 expression. (B) Coomassie stained SDS gel: 7 µg GST-Bet3 were incubated for 4h at room temperature with different concentrations of thrombin.

3 – 5 g *E.coli* cells were sonicated, cell debris removed by centrifugation and the cytosol applied to a 5 mL GSTrap FF column (flow rate 0.5 ml/min). After washing with PBS buffer the bound protein was cleaved overnight on the column with 100 U thrombin. The free Bet3 was eluted through a 1 mL HiTrap Benzamidin column (0.5 mL/min, 2 mL fractions) which removes thrombin (see fig. 4.2 A). The fractions containing protein were

pooled. Buffer exchange to PBS and concentration were achieved by ultrafiltration (Amicon Ultra concentrator, 10 kDa MWCO). Protein purity was verified by SDS-PAGE. The Coomassie stained gel showed only traces of impurity (see fig. 4.2 B).

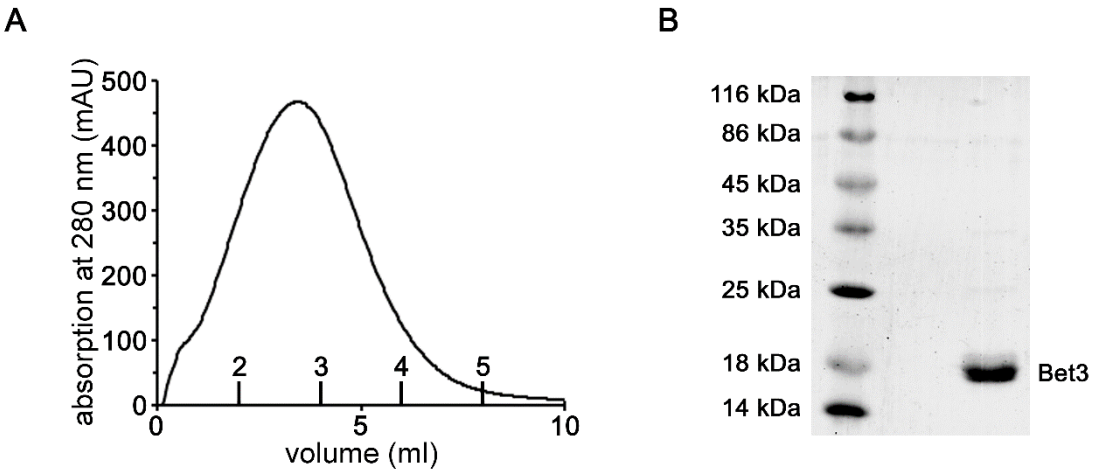

Figure 4.2: (A) Typical Bet3 purification elution profile including fractions. (B) SDS gel of purified Bet3.

4.2 Creation of Bet3 mutant A82V A136V through point mutation

To investigate membrane binding and the palmitoylation of Bet3 the following mutants were already available:

- Bet3 C68S and C68A in which the cysteine on which the palmitate chain is covalently bound is replaced and thus palmitoylation of the protein is inhibited.
- Bet3 KKEE in which the lysines K13 and K84 have been replaced with glutamic acid, disrupting the positively charged patch on the protein surface and thus suppressing possible electrostatic binding to the membrane.
- Bet3 A82L and A82V in which the alanine, lining the hydrophobic tunnel, has been replaced with a bulkier amino acid thus narrowing the tunnel to inhibit insertion of a fatty acid.

However, the mutants A82V and A82L, in which the hydrophobic tunnel is at least partly blocked, could still be palmitoylated, though with reduced efficiency. Bet3 A82V also showed in the crystal structure a fatty acid chain inside the tunnel [18], indicating that the tunnel is not completely blocked by the mutation.

For this reason, a double AAVV mutant with a completely blocked tunnel was engineered. A138, which extends into the tunnel almost opposite to A82, was exchanged to valine in addition to the A82V mutation. The correct sequence of the new mutant A82V A138V was validated by PCR sequencing (GATC, Konstanz) and protein expression verified by Western blot.

Since the tunnel constriction in Bet3 A82V A138V might have caused structural instability and non-palmitoylated Bet3 is generally less stable, protein stability of the mutant was checked by CD spectroscopy to ensure that the loss of self-palmitoylation activity or membrane binding was not due to partial denaturation of the mutant. The CD spectrum of Bet3 wild-type and mutant was compared and neither showed signs of partial protein unfolding (see fig 4.3) indicating that the protein stability has not been unduly influenced by the mutation.

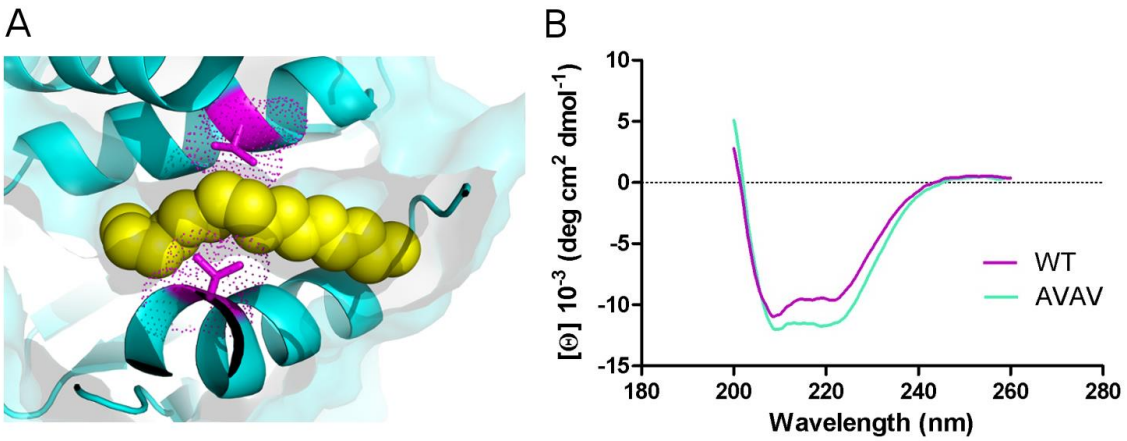

Figure 4.3: (A) Cartoon detail of the Bet3 A82V A138V structure showing the hydrophobic tunnel with the two mutated valines (pink, V138 top, V82 bottom). The electron densities of valines (purple dots) and of the palmitate chain (yellow) overlap indicating the steric blocking of the tunnel. Figure generated with PyMol, based on pdb 2CFH. (B) CD spectra of Bet3 wild-type and the tunnel-block mutant A82V A138V. Measurements were performed with a Jasco J720 spectropolarimeter at 20°C from 200 nm to 260 nm in a 0.2 cm path length cuvette.

Below the properties of all Bet3 variations used in this work are summarized:

	palmitoylated	open tunnel	positively charged patch
wild-type	yes	yes	yes
C68A / C68S	no	yes	yes
KKEE	yes	yes	no
A82V / A82L	partly	partly	yes
A82V A138V	no	no	yes

Table 4.1: Summary of the properties of the utilized Bet3 mutants.

4.3 Membrane binding of Bet3

4.3.1 Effects of different Bet3 mutations on membrane binding

The TRAPP complex acts as a tether in the vesicular transport between endoplasmic reticulum (ER) and Golgi and in yeast it localizes to the Golgi membrane [3]. Besides interaction with a membrane protein three possible membrane binding mechanism have been proposed based on the structural features of Bet3:

1. Insertion of the covalently bound fatty acid into the membrane.
2. Insertion of a membrane lipid fatty acid chain into the hydrophobic tunnel.
3. Electrostatic interaction between a positively charged surface patch of Bet3 and the negatively charged membrane surface.

So how does Bet3 bind to the membrane? Yeast cell viability tests gave no indication that the palmitoylation of Bet3 is critical for localization or function *in vivo* [17]. Experiments with HA-tagged Bet3 showed that a tunnel-blocking mutation as well as the exchange of lysines on its flat surface to glutamic acids were conditionally lethal. However, these findings could not be repeated with untagged Bet3 [4, 17]. Since the *in vivo* experiments had not been conclusive, two different *in vitro* assays were employed to further investigate membrane binding.

Most *in vitro* experiments were conducted using LUVs (large unilamellar vesicles) as a model for the cellular membrane. LUVs are liposomes of about 100 nm diameter and consist of a single lipid bilayer. Unless stated otherwise the LUVs were made from a lipid mixture similar to that of Golgi-membranes (50 % phosphatidylcholine (PC), 20 % phosphatidylethanolamine PE, 10 % phosphatidylinositol (PI), 10 % phosphatidylserine (PS) and 10 % cholesterol). For the flotation experiments 1 % of NBD-PC was added to allow for visual identification of the liposome containing fractions.

First membrane binding was investigated via a liposome flotation assay. Purified Bet3 (5 µM) was mixed with LUVs (1.25 mM lipids) and Nycodenz was added at final concentration of 40 %. Samples were overlaid first with buffer containing 30 % Nycodenz and then with buffer alone and centrifuged. During centrifugation the bound protein floats with the liposomes to the top of the gradient (see fig. 3.3). The advantage over simple liposome pelletation is the lack of false-positive results due to protein aggregation.

After centrifugation the liposome layer could be identified as a milky white, yellow fluorescent band on top of the gradient. Fractionation of the gradient in nine fractions top to bottom and SDS-PAGE revealed that the majority of all Bet3 molecules floated to the top of the gradient (see fig. 4.4 A). In contrast to integral membrane proteins, which are usually present only in the uppermost, membrane containing fraction [33], Bet3 was detected mainly in the upper three fractions, but spread to a lesser degree across the whole gradient. This might indicate that membrane binding of Bet3 is not stable, but a transient and dynamic event. This is in accordance with the observation that mammalian Bet3 exist in an unbound, cytosolic form [9]. In contrast, in the absence of LUVs Bet3 remained at the bottom of the gradient. Based on this result, Bet3 molecules present in the lower three fractions were defined as unbound protein, whereas Bet3 present in the upper six fractions is considered to possess membrane-binding activity.

Since Bet3 with and without GST tag showed similar flotation behavior, further experiments with different Bet3 mutants were performed with GST-tagged protein, since the GST tag increases protein stability [18]. Quantification of the density of the bands in each fraction was performed with the program Bio1D from PeqLab *(*see fig. 4.4 B*).*

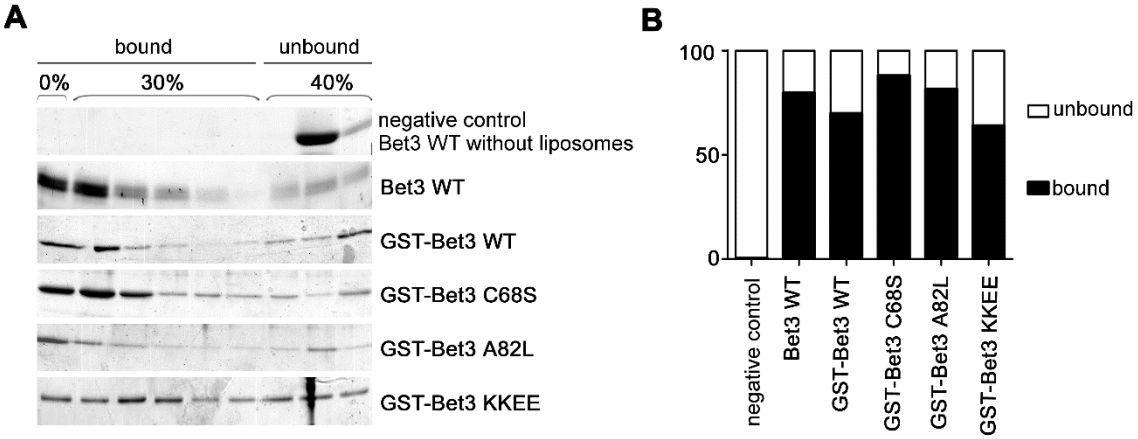

Figure 4.4: (A) Coomassie-stained SDS gel bands of flotation density gradients. GST-Bet3 was incubated with liposomes (50 % PC, 20 % PE, 10 % PS, 10 % PI, 10 % cholesterol). Then 40 % (w/v) Nycodenz were added and the mixture overlaid with buffer with 30 % and 0 % Nycodenz. During centrifugation liposome bound Bet3 floated to the top of the gradient, whereas unbound protein remained at the bottom. After centrifugation the gradient was divided in nine fraction top to bottom and analyzed by SDS PAGE. Bet3 without liposomes added served as negative control. (B) Since Bet3 liposome binding seems to be a dynamic process and therefore the protein was smeared across the gradient, the upper six fractions were defined as bound and the lower three fractions as unbound Bet3. To allow for comparison between different mutants the intensity of the SDS gel protein bands (see A) was quantified and plotted. Neither lack of palmitoylation, blocking of the hydrophobic tunnel nor suppression of electrostatic interactions alone, could abolish membrane binding.

Quantification of the density of the SDS gel bands showed that about 80 % of wild-type Bet3 was membrane bound. Similar values were obtained for the Bet3 mutants C68S

and A82L. Therefore it can be concluded that as expected [4] neither suppression of palmitoylation nor blocking of the hydrophobic tunnel alone affect membrane binding. The KKEE mutant with suppressed electrostatic interaction also showed membrane binding. However, the protein was spread more evenly across the gradient indicating a less stable binding than the wild-type.

Due to the dynamic nature of the Bet3 membrane interaction the flotation assay was difficult to quantify. Therefore, quantification via fluorescence anisotropy was attempted. If a fluorophore is excited with polarized light the emitted light is polarized as well, but if the fluorophore is rotating the orientation of the polarization plane will change depending on fluorescence lifetime and rotational speed. Since the rotational speed is dependent on the molecule size, binding of Bet3 to liposomes can be observed by measuring the anisotropy of the intrinsic tryptophan fluorescence.

To determine the anisotropy, the fluorophores are excited with vertically polarized light and the emission is detected with polarization filters vertical (I_{VV}) and horizontal (I_{VH}) to the excitation polarization plane. The anisotropy (r) is defined as:

$$r = \frac{I_{VV} - G I_{VH}}{I_{VV} + 2G I_{VH}}$$

with G an intrinsic instrument parameter compensating for the polarization plane angle dependent sensitivity of the emission monochromator.

A tenfold surplus of binding sites is required to ensure that every protein is bound to a liposome, in the case of Bet3 binding to LUVs this is equivalent to about 100 lipids per protein molecule (see chapter 3.4.3). On the other hand, to avoid light scattering, the liposome concentration should be as low as possible. Unfortunately, the intensity of the intrinsic tryptophan fluorescence of 0.1 µM Bet3 was too low so that the signal was lost in the background. The minimum required Bet3 concentration was determined to be 10 µM (data not shown).

The basic anisotropy of Bet3 in buffer was determined (r = 0.13) and then the lipid concentration increased in 20 µM steps. Bet3 wild-type showed an anisotropy increase up to r = 0.3. Upon addition of Triton X-100, which dissolves the liposomes, the anisotropy dropped back to the original value indicating specific Bet3 liposome interaction (see fig. 4.5 A). It was not possible to indefinitely increase the liposome concentration because above 100 µM the measured anisotropy values would exceed r = 0.4 clearly indicating disturbance by light scattering. An additional negative control with the non-membrane binding DNase only showed a slight increase in anisotropy due to light scattering. It can be concluded that the observed anisotropy increase is indeed caused by Bet3 liposome interaction, but due to the limitations through light scattering a quantitative analysis of K_D values was not possible.

Even though the measurements could not be quantified, qualitative comparisons between different Bet3 mutants were attempted. Because the measured anisotropy change varied between different liposome preparations, probably due to variations in the final lipid concentration, comparative measurements were always carried out with the same liposome preparation. As expected from the flotation assay no substantial difference in the binding properties of Bet3 wild-type, Bet3 C68A and the KKEE mutant could be detected (see fig. 4.5 B).

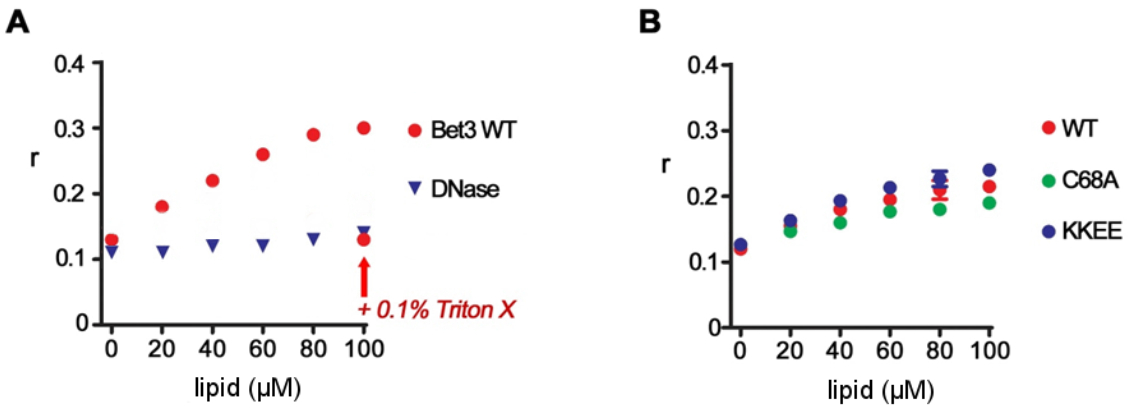

Figure 4.5: (A) Change of Bet3 anisotropy upon interaction with liposomes. Bet3 was titrated with liposomes mimicking the Golgi membrane. The increase in anisotropy indicates an increase in the apparent mass of Bet3 due to binding to a liposome. Upon addition of the liposome dissolving detergent Triton X-100 the anisotropy dropped to its original value. Non-membrane binding DNase was used as a negative control. (B) Anisotropy change of several Bet3 mutants upon titration with liposomes. As the flotation experiments had already indicated, neither lack of palmitoylation nor suppression of electrostatic interaction alone can abolish membrane binding.

Another approach to quantify Bet3 membrane binding was through quenching of the intrinsic tryptophan fluorescence upon interaction with SUVs (small unilamellar vesicles). Bet3 contains a single intrinsic fluorophore (W96) located on the protein surface in the proximity of the tunnel entrance. Upon excitation at 295 nm Bet3 shows a broad emission signal between 330 nm and 360 nm (see fig. 4.7 A).

Even though the use of GST-Bet3 would have been preferable due to the higher stability, untagged Bet3 was chosen because the GST tag also contains several tryptophans which are not quenched to an equal degree. This would have resulted in reduced sensitivity of the assay and would have made data analysis more difficult (see fig.4.6).

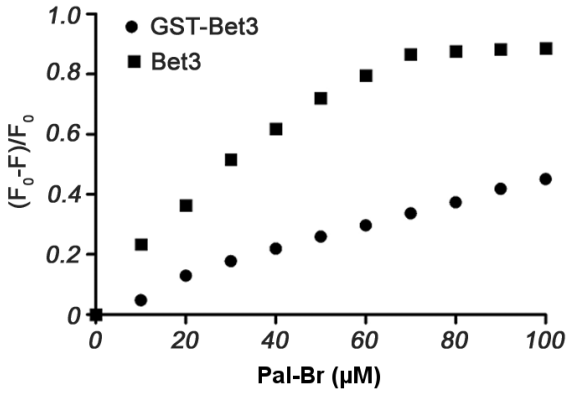

Figure 4.6: Influence of the additional tryptophans in the GST tag on fluorescence quenching upon titration with long chain fatty acids showing that the additional tryptophans in the GST tag reduced the assays sensitivity. Therefor all quenching experiments were performed with untagged Bet3.

Bet3 wild-type (see fig. 4.7 A) and the tunnel blocking mutant A82V A138V (see fig.4.7 B) were titrated with SUV stock solution and the change in tryptophan fluorescence detected.

Since the SUV stock solution contained fluorescing detergent which disturbed the measurement, the rising fluorescence in dependence of lipid concentration (see fig. 4.7 C) was determined and subtracted. Then the relative change in fluorescence intensity at 340 nm was plotted against the lipid concentration and analyzed with:

$$y = \frac{Y_{max} \cdot x}{K_D + x}$$

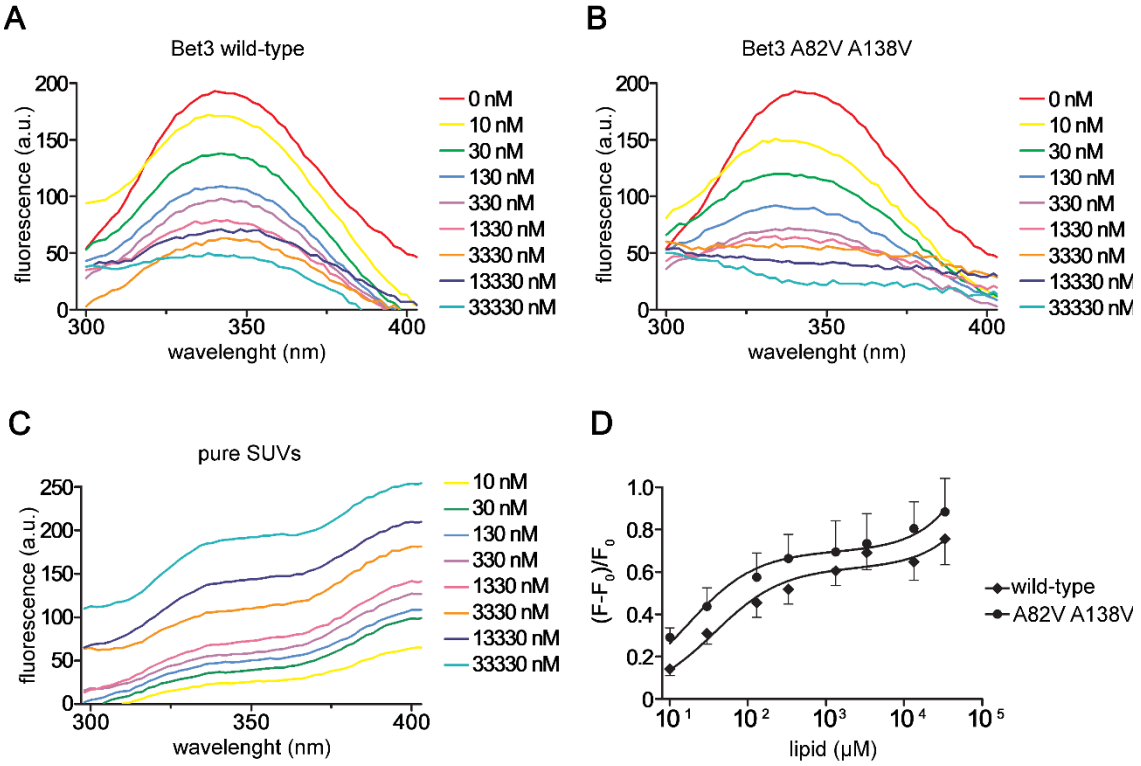

Figure 4.7: Quenching of the intrinsic tryptophan fluorescence of Bet3 wild-type (A) and tunnel blocking mutant Bet3 A82V A138V (B) upon titration with SUVs. (C) Because the SUV stock solution contained detergent, which fluoresces at 340 nm, the intrinsic fluorescence of the stock solution was determined and subtracted from the measured tryptophan fluorescence. (D) The relative change in fluorescence intensity at 340 nm was plotted against the lipid concentration and the K_D value of Bet3 wild-type was determined as 37±1 µM and of Bet3 A82V A138V as 17±1 µM, showing that even a completely blocked tunnel did not abolish membrane binding.

The K_D value of Bet3 wild-type was determined as 37±1 µM and of Bet3 A82V A138V as 17±1 µM (see fig. 4.7 D) showing that even a completely blocked tunnel did not abolish membrane binding. Since all evidence indicated that membrane binding could not be pinned to a single mutation and because the small SUV (ø 20-50 nm) might not be an appropriate membrane model due to their high curvature these experiments were not repeated with the other Bet3 mutants.

The successful binding of purified Bet3 to protein-free model membranes proved that Bet3 needs no protein partner to bind to membranes. Regarding the membrane binding mechanism, it can be stated that suppression of palmitoylation, blocking of the hydrophobic tunnel and removal of the positively charged patch all led to a reduction in membrane binding, but neither mutation could completely abolish the interaction with liposomes. Therefore it is suggested that membrane binding is achieved by weak binding forces of all three proposed binding mechanisms which together are strong enough to bind Bet3 to the membrane.

4.3.2 Influence of the lipid composition on Bet3 membrane binding

Bet3 is involved in the recruitment of ER-derived vesicles to the Golgi and each organelle membrane has its specific lipid composition. So is Bet3's localization mediated by the membrane's lipid composition? And do specific lipids enhance membrane binding or are they required at all?

To test the influence of the membrane's lipid composition several LUVs of varying composition were examined (see table 4.2).

LUV	Composition
LM-LUV (lipid mix)	10 % PI, 10 % PS, 10 % Chol, 20 % PE, 50 % PC
PC-LUV	100 % PC
PI/PS-LUV	10 % PI, 10 % PS, 80 % PC
Chol-10-LUV	10 % Chol, 90 % PC
Chol-40-LUV	40 % Chol, 60 % PC

Table 4.2: Composition of LUVs

The binding of Bet3 to PC-, PI/PS- and Chol-10-LUVs was examined with a liposome flotation assay. Fractionation of the gradient revealed that binding of GST-Bet3 wild-type to PC-LUVs is reduced compared to LM-LUVs (see fig. 4.8 and 4.4) and the protein floated only to the lower fractions of the gradient. Using PI/PS-LUVs also resulted in reduced Bet3 membrane binding, indicating that electrostatic interactions are not the predominant force. In contrast, 10 % cholesterol in the liposome (Chol-10-LUV) enhanced binding and also restored floatation of Bet3 to the upper fractions of the gradient.

The non-acylated mutant GST-Bet3 C68A also showed reduced binding to PC-LUVs and PI/PS-LUVs (see fig. 4.8). However, binding to Chol-10-LUVs was likewise not increased, suggesting that the exchange of the palmitoylation site reduced the preference of Bet3 for liposomes containing cholesterol.

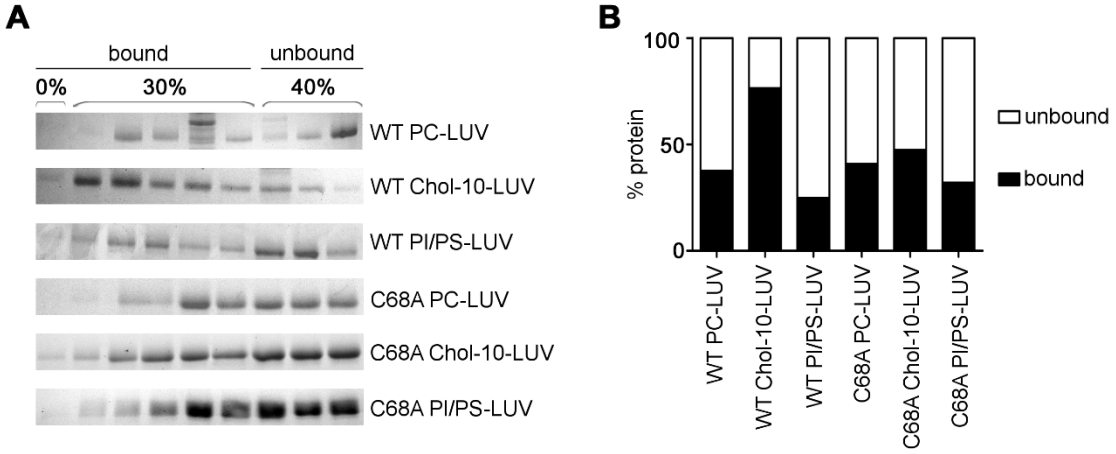

Figure 4.8: (A) Coomassie-stained SDS gel bands of flotation density gradients with liposomes of different composition (compare table 4.2). After centrifugation the gradient was divided top to bottom in nine fractions and analyzed by SDS PAGE. The upper six fractions were defined as bound and the lower three fractions as unbound Bet3. (B) Graphic visualization of the intensity of the protein bands of the SDS gel. Binding of Bet3 wild-type to LUVs made only from PC was reduced, but could be resurrected by 10 % cholesterol, though not by adding charged phospholipids. With un-palmitoylated mutant Bet3 C68A the binding enhancing effect of cholesterol was only very slight, suggesting that the exchange of the palmitoylation site reduced the preference of Bet3 for liposomes containing cholesterol.

The lipid binding specificity of Bet3 was further investigated with the fluorescence anisotropy assay. Adding increasing amounts of LM-, PC- and PI/PS-LUVs to Bet3 wild-type increased the anisotropy to (almost) identical values indicating a similar affinity of the respective liposomes to Bet3 (see fig. 4.9 A). Only Chol-10-LUVs yielded higher r-values confirming the results from the floatation assay. However, increasing the cholesterol content further to 40 % (Chol-40-LUV) reduced membrane binding below that of all other LUVs. Thus, cholesterol had a stimulatory effect at low concentrations but an inhibitory effect at higher concentrations.

Similar results were obtained for Bet3 C68A (see fig. 4.9 B). Chol-10-LUVs exhibited the highest r-values, whereas Chol-40-LUVs revealed the lowest r-values. However, the stimulatory effect of cholesterol was less pronounced for Bet3 C68A compared to Bet3 wild-type. This is also in line with the results obtained from the floatation assay.

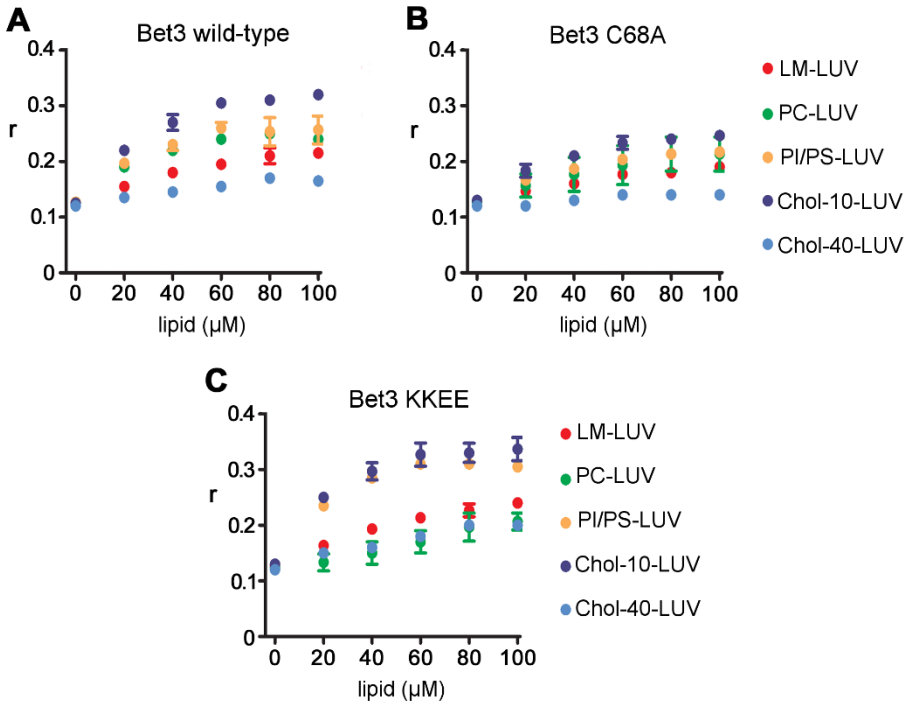

Figure 4.9: Anisotropy changes of Bet3 wild-type (A), un-palmitoylated Bet3 (B) and a mutant suppressed electrostatic interaction (C) upon interacting with liposomes of different compositions (compare table 4.2). For all three mutants the anisotropy value was highest for liposomes containing 10 % cholesterol, a concentration typical for the Golgi membrane. However, increasing the cholesterol content further to 40 % reduced membrane binding below that of all other LUVs. The second strongest binding was in all cases to PI/PS-LUVs. Compared to the wild-type the effects were less pronounced for Bet3 C68A and stronger for Bet3 KKEE.

Finally, the lipid binding preferences of Bet3 KKEE, in which a possible electrostatic interaction through surface lysines is suppressed, were investigated. Bet3 KKEE did associate with LUVs of all compositions but it showed a lipid preference distinct from the wild-type protein (see fig. 4.9 C). Chol-10-LUVs caused the highest increase in anisotropy. Almost identical high r-values were obtained with PI/PS-LUVs. Binding was again reduced when using Chol-40-LUVs.

In summary it can be stated that Bet3 membrane binding was most affected by the presence of cholesterol. With 10 % cholesterol, a concentration in the 10-15 % range typical for the Golgi membrane [34-37], enhancing membrane binding. On the other hand 40 % cholesterol, a concentration typical for the plasma membrane, had an adversary effect [36-38].

4.4 Palmitoylation of Bet3

In contrast to other proteins that require an acyl-transferase for palmitoylation, Bet3 is palmitoylated through an auto-catalytic reaction with Pal-CoA as the lipid substrate [18]. Palmitoylation occurs via a S_N2 reaction at cysteine 68, which is located at the outer end of the hydrophobic tunnel. Since the attempt to determine the substrate binding site of Bet3 by co-crystallization with Myr-X-CoA, a non-hydrolysable acyl-CoA, had been unsuccessful [25], an alternative fluorescence spectrometric approach was chosen to further define the substrate binding site of Bet3.

4.4.1 Binding of acyl-CoAs and palmitoylation inhibitors to Bet3

Experiments with purified protein have shown that Bet3 can also be acylated with fatty acids other than Pal-CoA [25]. This lead to the question: can further information about the substrate binding site be gained from the quantification of the interaction of Bet3 with acyl-CoAs of different length and shape?

For this purpose, the respective acyl-CoAs were added to 10 µM Bet3 in 25 µM steps (in the case of octanoyl- and acetyl-CoA in 1mM steps) and the intrinsic tryptophan fluorescence was monitored. The fluorescence intensity was plotted against the substrate concentration (see fig. 4.10) and the K_D calculated as described in chapter 3.4.1.

For long chain fatty acids (14-18 carbon atoms) K_D values between 1.3 µM and 2.0 µM were calculated while short chain fatty acids showed almost no binding to Bet3 displaying K_D values over 7000 µM (see table 4.3). From the fact that stearoyl-CoA and oleoyl-CoA showed similar K_D values it can be deduced that substrate binding is not influenced by the kink in the fatty acid chain.

To ensure that the change in fluorescence intensity is caused by initial substrate binding and does not depend on covalent binding of the fatty acid, Bet3 wild-type was also tested with the palmitoylation inhibitor 2-bromopalmitate [39] and the non-hydrolysable myristyol-CoA derivative Myr-X-CoA, in which fatty acid and CoA are linkend by a thioether bond. Their K_D values lay in the same range as those of the other long chain acyl-CoAs (1.3 µM and 3 µM; see table 4.3) indicating that the quenching is solely caused by substrate binding.

Acyl-CoA	# C-atoms	Bet3 wild-type	Bet3 C68A
Stearoyl-CoA	18	1.3 ± 0.8	2.9 ± 0.8
Oleoyl-CoA	16	2.1 ± 0.6	1.1 ± 0.3
Palmitoyl-CoA	16	1.8 ± 0.7	1.6 ± 0.6
Myristoyl-CoA	14	2.0 ± 0.8	2.3 ± 1.6
Octanoyl-CoA	8	7252 ± 1412	11256 ± 3055
Acetyl-CoA	2	7624 ± 2110	7321 ± 1327
2-bromopalmitate	16	1.3 ± 0.5	1.9 ± 0.3
Myr-X-CoA	14	3.0 ± 0.6	

Table 4.3: K_D values of different acyl CoAs binding to Bet3 wild-type and Bet3 C68A.

This result was confirmed by repeating the assay with the mutant Bet3 C68A, in which the acylation site C68 has been exchanged to alanine. The measured K_D values lie in the same range as those of Bet3 wild-type (see table 4.3).

Wild-type Bet3 and Bet3 C68A have identical affinities for the substrates, indicating that binding and fatty acid transfer are distinct events. The length of the acyl chain is relevant, as long chain acyl-CoAs ($\geq$ 14 carbon atoms) showed a thousand times stronger affinity than short chain acyl-CoAs ($\leq$ 8 carbon atoms), but a kink in the fatty acid does not affect binding, since oleoyl-CoA binds with similar K_D as Stear-CoA and Pal-CoA.

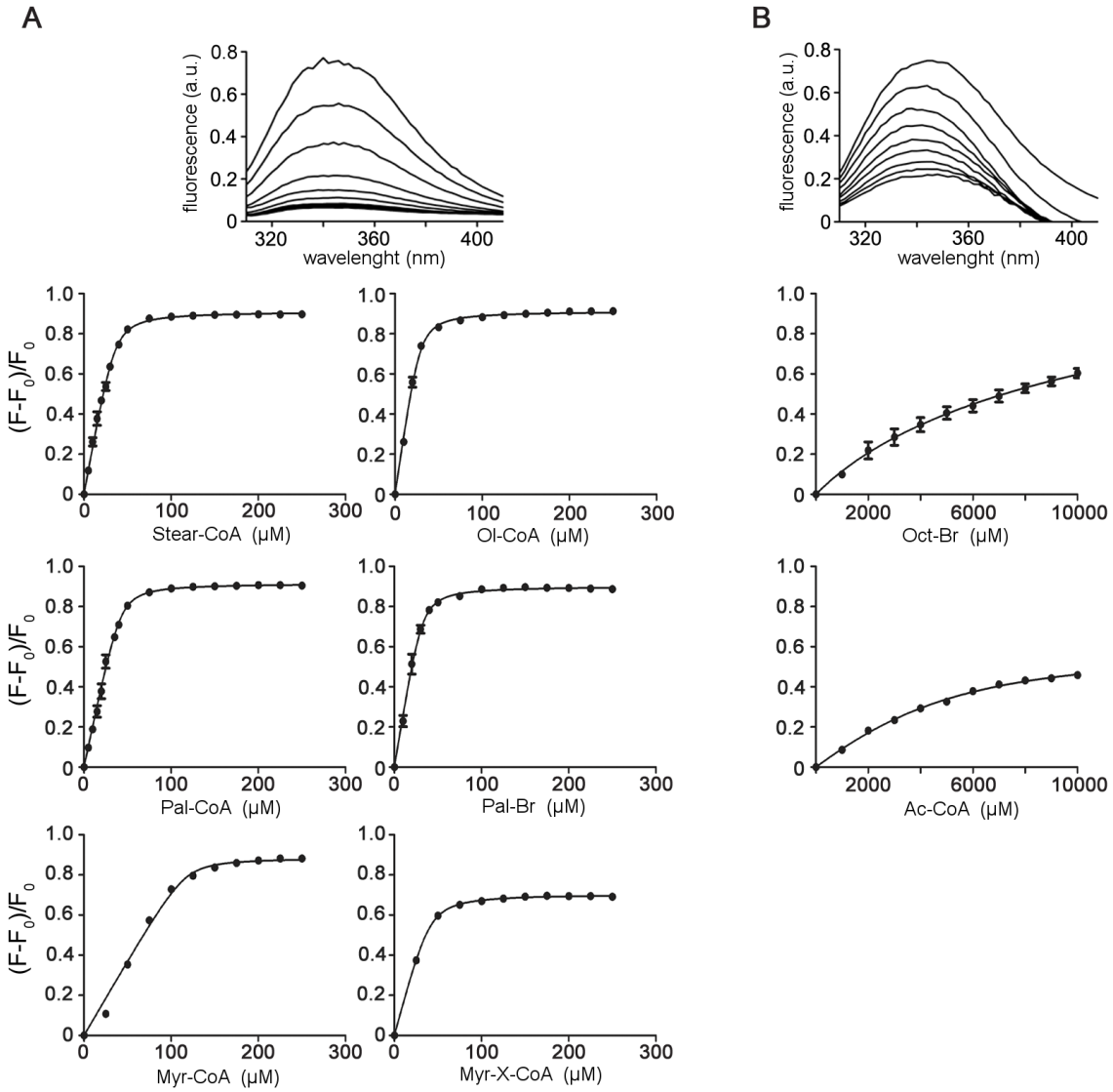

Figure 4.10: Fluorescence quenching of Bet3 wild-type upon titration with long chain (A) and short chain (B) acyl CoAs. In the top panel exemplary spectra of titration with Pal-CoA (A) and Ac-CoA (B) are shown. The fluorescence intensity maximum is at 340 nm**.** Below the change in fluorescence intensity at 340 nm is plotted against the substrate concentration. Each measurement was repeated three times. The standard deviation is shown by error bars. If the error bars are invisible, it is because they are smaller than the symbol. Long chain fatty acids all show binding to Bet3, even the palmitoylation inhibitor 2-bromopalmitate and the non-hydrolysable myristoyl CoA derivative Myr-X-CoA, indicating that binding is an independent step taking place before the fatty acid transfer (K_D values between 1.3-3.0 µM). Short chain fatty acids show a thousandfold reduced binding activity (K_D values over 7000 µM). All K_D values are summarized in table 4.3.

4.4.2 Localization of the substrate binding site

The other interesting question was: where does the substrate actually bind? It has been suggested that the substrate binds by insertion of the fatty acid into the tunnel of Bet3 [18].

To test this hypothesis, the fluorescence quenching assay as described above was employed to monitor the binding of Pal-CoA to the three Bet3 mutants: C68A (suppressed covalent binding), A82V (partially blocked tunnel) and A82V A138V (completely blocked tunnel).

The K_D values of Bet3 wild-type and Bet3 C68A were almost identical, the K_D value of Bet3 A82V only slightly increased (see table 4.3). Surprisingly the calculation of binding sites (see chapter 3.4.1.) indicated not only one but three substrate binding sites for all three proteins.

The mutant Bet3 A82V A138V showed Pal-CoA binding with an increased K_D value (15.8 µM) and only two binding sites, indicating that indeed one binding site is the hydrophobic tunnel (see fig. 4.11 A). Furthermore, a palmitoylation assay with [^{3}H]-Pal-CoA resulted in no self-palmitoylation (see fig. 4.11 B). Thus it can be concluded that the insertion of the fatty acid into the tunnel is a requirement for the self-palmitoylation of Bet3.

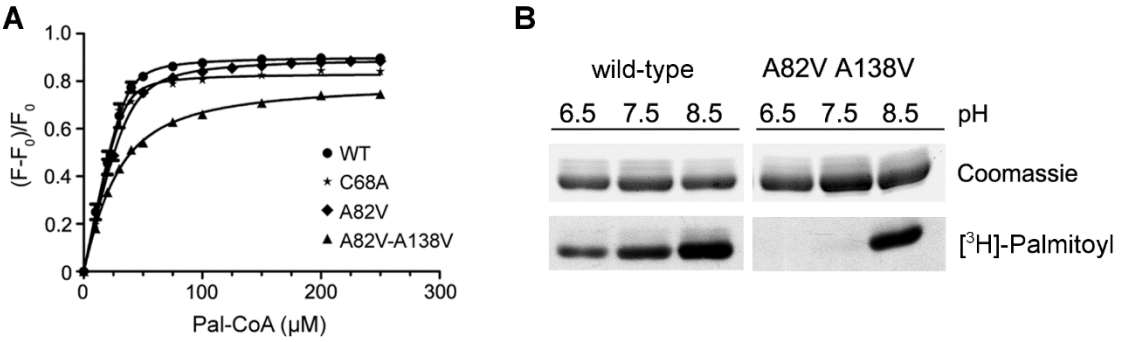

Figure 4.11: (A) Relative change in fluorescence intensity of different Bet3 mutants upon titration with Pal-CoA. Each measurement was repeated three times. The standard deviation is shown by error bars. If the error bars are invisible, it is because they are smaller than the symbol. The calculated K_D values and number of binding sites are listed in table 4.4. (B) Palmitoylation of Bet3 A82V A138V with [^{3}H]-Pal-CoA. The protein was incubated at different pH values with radioactive Pal-CoA, and the acylated protein then documented by fluorographic detection after SDS-PAGE. Bet3 A82V A138V showed no self-palmitoylation activity at neutral pH, therefore the insertion of the fatty acid into the tunnel is a requirement for the self-palmitoylation of Bet3.

Bet3 mutant	K_D	# binding sites
Wild-type	1.8 ± 0.7	3.5 ± 0.2
C68A	1.6 ± 0.6	3.3 ± 0.2
A82V	4.0 ± 0.5	3.7 ± 0.1
A82V-A138V	15.8 ± 2.3	2.1 ± 0.4

Table 4.4: K_D values and number of binding sites of Pal-CoA binding to Bet3 wild-type and several Bet3 mutants. Bet3 wild-type as well as the Bet3 mutants C68A and A82V have not only one but three palmitoyl binding sites. The mutant Bet3 A82V A138V, in which the hydrophobic tunnel is completely blocked, has only two binding sites. Therefore, it can be concluded that one palmitoyl binding site is the hydrophobic tunnel, but that there are additional binding sites on the Bet3 surface.

One way to uncover the location of the two additional binding sites would be to co-crystallize the protein with substrate. However, efforts to co-crystallize Bet3 C68A with Myr-X-CoA had been without success because the substrate was expelled from the crystal during crystallization [25]. Therefore, 2D ^{15}N NMR and 3D ^{15}N, ^{1}H and ^{13}C triple resonance through bond spectra of a Bet3 C68A/TrappC6 dimer were recorded, either alone or in the presence of CoA or Pal-CoA (see fig. 4.12).

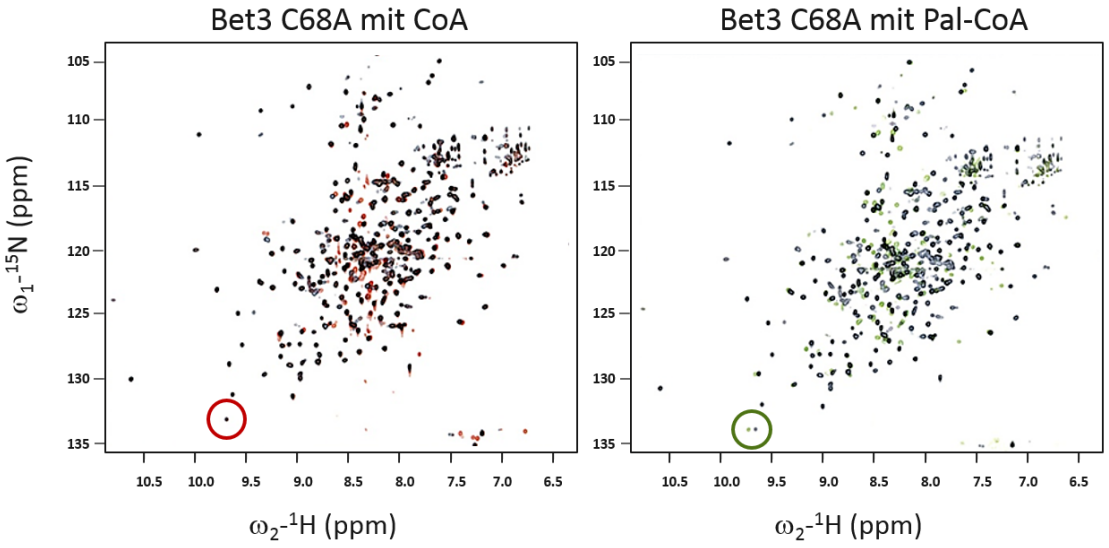

Figure 4.12: 2D NMR spectra of Bet3 C68A/TrappC6 without a ligand (black), with CoA (red) or Pal-CoA (green). All amino acids that are influenced directly or indirectly by interaction with the substrates show colored shifts. Measurements were kindly performed by Dr. Daniel Kümmel (AG Heinemann, Max Delbrück Center for Molecular Medicine (MDC), Berlin) in co-operation with Dr. Peter Schmieder (Leibniz-Institut für Molekulare Pharmakologie (FMP), Berlin). Data analysis was performed with the soft-ware of the Collaborative Computational Project for NMR (CCPN).

During the recording of the NMR spectra the first ten amino acids of the N-terminus were partially cleaved resulting in blurred spectra and in parts in fused peaks. This prevented the full analysis of the NMR data. In total 62 % of all amino acids and 79 % of all shifted amino acids could be identified.

Two separate areas of amino acids, shifted in the presence of Pal-CoA, could be identified on the Bet3 surface (see fig. 4.13). Both areas consist of mostly hydrophobic amino acids, indicating a hydrophobic interaction with the fatty acid. Additionally, amino acids in the loops between the helices α1 and α2 and the between the β-sheet β4 and the helix α4 shifted in the presence of Pal-CoA.

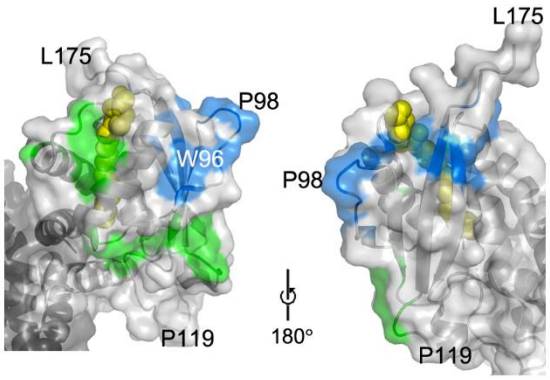

Figure 4.13: Areas of hydrophobic amino acids which might interact with the fatty acid of the substrate. The green area includes amino acids L60, A61, V65, G66, V77, V81, L87, G88, I89, I106, L107, P111, G159 and V160; the blue area the amino acids F71, I93, W96, P98, A99, G100, A145, F167, I168 and I171. Figure generated with PyMol, pdb 2CFH.

Bet3 has not only one, but three substrate binding sites which all bind Pal-CoA with similar affinity. One binding site is as expected inside the hydrophobic tunnel, in addition two hydrophobic patches on the protein surface probably also bind Pal-CoA. The purpose of these binding sites might be to extract Pal-CoA from organelle membranes prior to insertion of the fatty acid into the hydrophobic tunnel.

5 Discussion

5.1 Membrane binding of Bet3

To fulfill its tethering function, the TRAPP complex in some way has to interact with the vesicular carriers as well as the organelle membrane. Previous studies showed that TRAPP via its Bet3 subunit interacts with the Sec23 subunit of COPII coats of vesicles in the ER-to-Golgi transport [4]. On the organelle side the situation is less clear. It has been shown that Bet3 binds tightly to Golgi membranes in yeast, where it cannot be extracted from cellular membranes by high salt or carbonate, but requires detergent for solubilization [7, 16]. Bet3 is also at least transiently membrane bound in mammalian cells [9]. However, no protein interaction partner like Sec23 has been identified to date at the Golgi (or IC) membrane. In this work LUVs were used as artificial membrane models and it could be shown by liposome flotation assays that no other protein is needed to achieve transient membrane binding of human Bet3.

Several mechanisms for membrane binding have been suggested: the insertion of the covalently bound palmitoyl chain into the lipid bilayer of the membrane and/or the insertion of a lipid chain from the membrane into the hydrophobic tunnel, and thirdly, electrostatic binding via a positively charged patch on the Bet3 surface. However previous *in vivo* experiments with yeast mutants have produced inconsistent results [4, 17]. Therefore, membrane binding was investigated *in vitro* using LUVs and the Bet3 wild-type and the mutants Bet3 C68A / Bet3 C68S (no covalent palmitoylation), Bet3 A82L / Bet3 A82V A138V (blocking of the hydrophobic tunnel) and Bet3 KKEE (removal of the positively charged patch).

Liposome flotation assays showed a membrane binding of about 80 % of Bet3 wild-type. However, the protein was not concentrated in the uppermost density gradient fraction containing the liposomes, but instead spread over several fractions suggesting dynamic membrane binding. This observation is in accordance with the observation that only 15 % of mammalian Bet3 are tightly membrane bound, whereas the remainder is recruited to the membrane in a dynamic manner [9]. The Bet3 mutants C68S, A82V and KKEE showed similar levels of membrane binding (compare fig. 4.4 B).

Because the dynamic nature of membrane association made the quantification of the flotation assay difficult another approach was utilized using the change in fluorescence anisotropy of the intrinsic tryptophan upon binding to liposomes. Bet3 C68A and Bet3 KKEE showed slightly reduced levels of membrane binding compared to the wild-type (compare fig. 4.5 B). Light scattering by the liposomes prevented quantification as well. To investigate the effect of tunnel blocking a third method, quenching of the intrinsic tryptophan fluorescence, was employed. Again a reduction of membrane binding (K_D values of 17±1 µM for A82V A138V vs. 37±1 µM for the wild-type) but no complete abolition could be observed (compare fig. 4.6 D). It is therefore proposed that the binding of Bet3 is mediated by several weak interactions which in combination achieve a strong interaction force (see fig. 5.1). One of these regions on its own might not be sufficient to sustain membrane binding, and the abolition of only one of these regions might hence not eliminate membrane association of the complete protein.

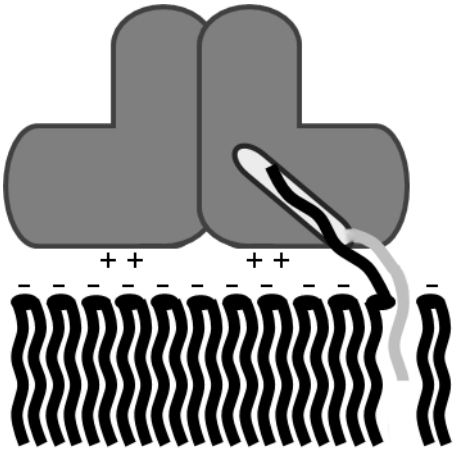

Figure 5.1: Model of Bet3 membrane binding through the synergistic effect of weak protein membrane interactions. Insertion of the covalently bound palmitate into the membrane, insertion of a fatty acid chain from the lipid bilayer into the hydrophobic tunnel and electrostatic interaction between protein and membrane surface all contribute to Bet3 membrane binding.

The membrane binding of Bet3 and its mutants was investigated using LUVs with a lipid composition which crudely mimics the Golgi membrane (LM-LUVs). Next the influence of the lipid composition on Bet3 membrane binding was examined. The liposome flotation assay showed that Bet3 wild-type binding had been halved for PC- and PI/PS-LUVs (compare table 4.2). Only liposomes containing 10 % cholesterol (Chol-10-LUVs) could retain the same Bet3 binding capacity as the original lipid mix (76 % bound). For Bet3 C68A binding to PC- and PI/PS-LUVs showed reduced binding with similar values as the wild-type and the binding of Bet3 C68A to Chol-10-LUVs was reduced to 50 % (compare fig. 4.8 B).

In addition, the interaction of Bet3 wild-type, Bet3 C68A and Bet3 KKEE with LM-, PC-, PI/PS-, Chol-10- and Chol-40-LUVs was investigated using fluorescence anisotropy (compare fig. 4.9). The results showed again the strongest binding of all Bet3 mutants to Chol-10-LUVs. The increase of cholesterol to 40 % did not further increase membrane binding. Instead Chol-40-LUVs caused the least change in fluorescence anisotropy indicating that while a low cholesterol content enhances membrane binding, high cholesterol levels have an adversary effect. The dependence on the cholesterol level might explain the localization of TRAPP I at the Golgi, since the Golgi membrane contains 10-15 % cholesterol, whereas the plasma membrane has a cholesterol content of 30-50 % [36-38].

The mechanism which allows the sensing of the cholesterol content is not clear yet and would require further research. The observation that the effect of cholesterol is notably reduced in the unpalmitoylated Bet3 mutant C68A, suggests an involvement of the palmitoyl chain in cholesterol recognition. Indirect immuno-fluorescence imaging of HA-tagged Bet3 showed no mislocalization of a C68S mutant *in vivo*, but a later study using untagged Bet3 suggested that the Bet3 localization might have been influenced by the HA tag [4, 17]. On the other hand palmitoyl is known to interact with cholesterol and palmitoylation is often a signal for the localization of proteins to membrane domains enriched in cholesterol, called lipid rafts [40]. This effect has been shown for many transmembrane receptors and viral proteins with transmembrane domains as well as for peripheral proteins like e.g. members of the Ras GTPase family [19, 20, 40, 41]. However the exact mechanisms underlying the partitioning of proteins in lipid rafts are yet not fully understood as there are also examples known of palmitoylation causing the exclusion from lipid rafts, e.g. the protective antigen of the antraxin toxin [42]. Further research in the field of palmitoyl cholesterol interaction might result in an explanation for the apparent preference of Bet3 for membranes containing low levels of cholesterol.

An alternative explanation could be the existence of a cholesterol binding protein sequence. Cholesterol binding peptide sequences like the CRAC (cholesterol recognition/interaction amino acid consensus) motif (L/V-$X_{(1-5)}$-Y- $X_{(1-5)}$-K/R) have been found on transmembrane proteins [43]. Other cholesterol binding proteins showed similar motives, which also follow the pattern of “branched aliphatic amino acid – spacer amino acid – aromatic amino acid” [44, 45]. The branched aliphatic amino acid and the methyl groups on the cholesterol surface interdigitate and bind via van der Waals interactions. The aromatic acid interacts with cholesterol via π-orbital stacking of the aromatic rings [46]. On the long loop between β2 and α4 of Bet3 are two sequences

($_{112}$VDF$_{114}$ and $_{124}$LIY$_{126}$) located which follow this pattern and whose side chains are oriented towards the protein surface. If the loop would insert itself partly into the lipid bilayer cholesterol binding might ensue. This proposed binding mechanism is purely speculative, but it could be an alternative explanation for the observed binding behavior, especially since the CRAC peptide LWIYIK binds to cholesterol in model membranes with low cholesterol content (2.5 %) only, but showed no interaction at a cholesterol content of 40 % [47].

5.2 Substrate binding during self-acylation of Bet3

In the presence of Pal-CoA Bet3 is acylated by an autocatalytic mechanism. It has been proposed that insertion of the fatty acid into the hydrophobic tunnel is a necessary step in the catalytic mechanism, since this would position the thioester bond right at the tunnel entrance near C68. Then the palmitate chain could be transferred onto the cysteine by a nucleophilic attack of the cysteine's sulfur group on the thioester bond in Pal-CoA [18]. Palmitoylation assays with [^{3}H]-Pal-CoA showed that acyl-CoAs with long chain fatty acids ($\geq$ 14 carbon atoms) and palmitoylation inhibitors could suppress self-palmitoylation in the micromolar range, presumably by competing for the substrate binding site. Acyl-CoAs with short chain fatty acids ($\leq$ 8 carbon atoms), free palmitate and CoA did not inhibit the self-palmitoylation activity [25]. Since the attempt to determine the substrate binding site of Bet3 by co-crystallization with Myr-X-CoA, a non-hydrolysable acyl-CoA, had been unsuccessful [25], a fluorescence spectrometric approach was chosen to characterize the substrate binding site.

The intrinsic fluorescence of Bet3's only tryptophan, located near the tunnel entrance, is quenched upon the addition of long chain acyl-CoAs. The K_D values of Stear-CoA (18:0), Pal-CoA (16:0) and Myr-CoA (14:0) were determined as values between 1.3 µM and 2.0 µM (compare table 4.3). The concentration of Pal-CoA in cells is 5.7 µM [24], so the K_D of Bet3 substrate binding lies within the physiological concentration range. Oleoyl-CoA (16:1), containing one double bond in its fatty acid also bound with a K_D of 2.1 µM, indicating that a kink in the carbon chain does not diminish substrate binding. Unlike the long chain acyl-CoAs, acyl-CoAs with a short fatty acid chain did not display strong interaction with Bet3. The measured K_D values for Oct-CoA (8:0) and Ac-CoA (2:0) were both about 7 mM, which signifies a more than a thousand times weaker binding force (compare table 4.3). The palmitoylation inhibitors 2-bromopalmitate and Myr-X-CoA, both unable to bind covalently, showed K_D values similar to the long chain acyl-CoAs.

Hence it can be assumed that the observed fluorescence quenching is caused by the substrate binding step and seems to be independent of covalent substrate attachment.

Repeating the experiments with Bet3 C68A long chain acyl-CoAs and 2-bromopalmitate also bound with K_D values between 1.1µM and 2.9 µM, whereas the short chain acyl-CoAs again bound in the millimolar range (compare table 4.3). Thus wild-type Bet3 and Bet3 C68A have identical affinities to the lipid substrate, indicating that substrate binding and fatty acid transfer are distinct events.

The quantification of Bet3 substrate binding did not only confirm the relevance of the acyl chain length but also revealed the binding of three ligands instead of the expected one. To further test the assumption that at least one acyl-CoA binding site is the hydrophobic tunnel, Pal-CoA was added to Bet3 A82V and the fluorescence quenching quantified. However, Bet3 A82V still displayed threefold ligand binding and only a slightly lower K_D of 4.0 µM (compare table 4.4).

Since Bet3 A82V or A82L still show residual self-palmitoylating activity at neutral pH [18], it is likely that the mutation does not sufficiently restrict the tunnel to completely exclude insertion of a fatty acid. Therefore, an improved tunnel blocking mutant was engineered, in which alanine 138, which is located in the middle of the hydrophobic tunnel opposite to alanine 82, was also replaced by the bulky amino acid valine. Palmitoylation with [^{3}H]-Pal-CoA was completely blocked at neutral pH and CD spectroscopy indicated that the secondary structure of Bet3 was not changed by the mutation (compare fig. 4.11 B and fig. 4.3 B). At basic pH, Bet3 A82V-A138V is acylated, probably because the basic environment causes the tunnel to open thereby allowing the insertion of a fatty acid.

Determining the K_D value for the A82V A138V mutant revealed only a slight reduction in its affinity for Pal-CoA to 16 µM, indicating that it still binds efficiently to Pal-CoA (compare table 4.4). However, the number of calculated binding sites was reduced to two in this mutant containing a completely blocked tunnel. Palmitoylation with [^{3}H]-Pal-CoA as well as the fluorescence quenching assay both support the assumption that the hydrophobic tunnel is indeed a binding site for acyl-CoAs and that insertion of the fatty acid is a prerequisite for self-acylation. In addition, other substrate sites with similar affinity exist, probably at the surface of the molecule. 2D-NMR spectroscopy of the Bet3 C68A/TrappC6 dimer in the presence of Pal-CoA revealed two hydrophobic patches on the surface of Bet3 which might interact with acyl chains (compare fig. 4.13).

The purpose of the additional substrate binding sites might be to extract Pal-CoA from organelle membranes prior to insertion of the fatty acid into the hydrophobic tunnel. Despite a total cellular Pal-CoA concentration of about 5.7 µM, there is almost no free acyl-CoA available in the cytosol. Virtually all cytosolic acyl-CoA molecules exist in a complex with the cytosolic acyl-CoA binding protein (ACBP) which binds its ligand with nanomolar affinity [24]. Thus, acyl-CoAs are available only at intracellular membranes, such as the ER and the Golgi, where they are required for the synthesis of phospholipids and also for DHHC-catalyzed S-acylation of proteins [48, 49]. Since Bet3's intrinsic membrane binding activity targets the protein to the Golgi membrane [16, 17], it is conceivable that it gains its substrate from this membrane acyl-CoA pool. However, Bet3 probably does not penetrate deeply into the bilayer but resides at the membrane surface. So it would be difficult to interact with a fatty acid, which is embedded in the hydrophobic interior of the bilayer, if the only available substrate binding site was the hydrophobic tunnel inside the protein. Additional external binding sites at the protein surface might therefore facilitate the extraction of acyl-CoAs from the membrane.

If Pal-CoA is indeed extracted from the membrane by attachment to hydrophobic patches on the protein surface, how then can the palmitate chain be inserted into the tunnel? Bet3 shares structural similarities with the non-specific LTPs (lipid transfer proteins) from plants and mammals [16, 50-52]. Like Bet3, LTPs bind lipids in a hydrophobic tunnel which spans the protein. The hydrophobic carbon chain is buried inside the protein and the carboxyl or CoA group is localized at the aqueous interface in contact with surface residues and water molecules. Barley LTP can expand and contract its binding pocket according to the size of the bound fatty acid [51]. Upon binding of Pal-CoA the NMR solution structure of barley LTP showed a bending motion in its helix αA and structural adjustments of the C-terminus and helix αC to accommodate the fatty acid inside the tunnel [50].

A similar helix bending and rotation motion has been described for Bet3 [16]. Comparison of the structure of Bet3 with an empty tunnel and with the fatty acid embedded in the hydrophobic tunnel revealed a rotation of approximately 30° of the lower half (towards the tunnel entrance) of helix α2 about a hinge region close to G52, located near the middle of α2 [16]. This bending motion, with a maximal displacement of approximately 9 Å, would open the hydrophobic tunnel (see fig. 5.2 A). It has been suggested that in ligand-free, non-acylated Bet3 the helix α2 is rotated outwards, thereby opening up the tunnel. Induced by the binding of acyl-CoAs to the surface of Bet3 a conformational change may be triggered which allows helix α2 to rotate back to its original position

thereby inserting the acyl chain into the tunnel (see fig. 5.2 B). Narrowing or blocking the tunnel by introduction of bulky amino acids might therefore reduce acylation of Bet3 not only because the insertion of the fatty acid is sterically inhibited, but also because the conformational change which causes fatty acid insertion is hindered. The Bet3 structure displays within the putative hinge region an extended hydrogen-bonding pattern which must be modulated to allow movement of helix α2. Thus the conformational change might be sensitive to the pH, which would explain how a partial restriction of the tunnel can be complemented by a slightly basic pH [25].

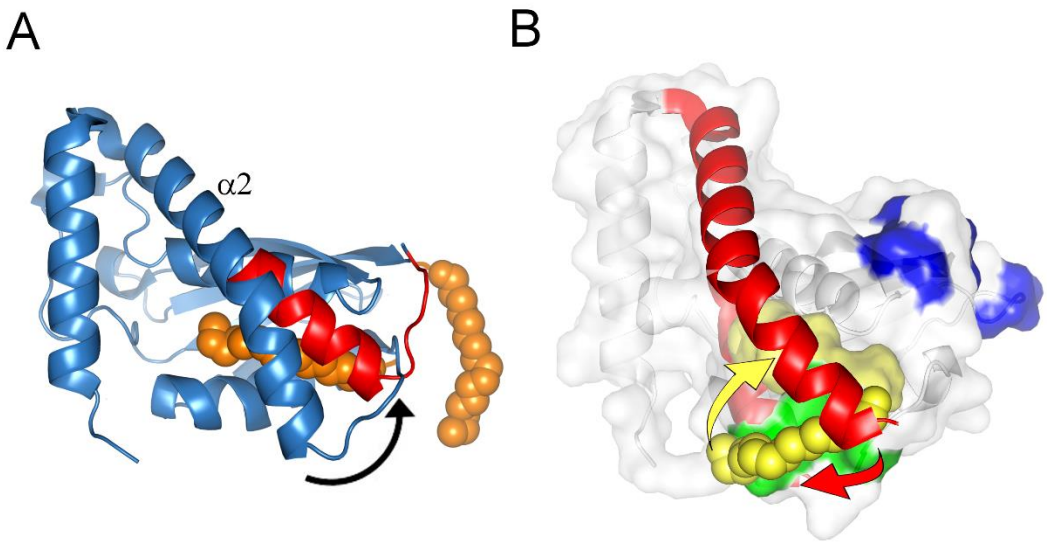

Figure 5.2: (A) Overlayed structures of Bet3 with the palmitate chain (orange) inside the tunnel (blue cartoon) and with the lower half of helix α2 rotated 30° (red) so that the tunnel is open and the palmitate can leave the tunnel. (B) Proposed mechanism for tunnel insertion of Pal-Co: helix α2 (red) rotates back to its original position (light red) thereby inserting the acyl chain (yellow) into the tunnel. The surface of the hydrophobic tunnel is depicted in light yellow. The surface substrate binding sites are indicated in blue and green. The cartoon of the protein structure was generated with PyMol, pdb 2CFH.

In summary, Bet3 self-palmitoylation requires the presence of Pal-CoA in the hydrophobic tunnel, with the fatty acid bound inside and the CoA group extending outside the protein. Two additional hydrophobic binding sites on the Bet3 surface were identified which might help to extract Pal-CoA from the organelle membrane. Surface bound Pal-CoA might then be transferred into the tunnel by conformational change. Upon insertion into the tunnel the palmitate chain is transferred to C68 via S-acylation.

6 Summary

6.1 Summary

In eukaryotic cells the transport along secretory and endocytic pathways is performed by vesicular carriers. The initial attachment of a vesicle to the target membrane is called tethering. In case of ER-to-Golgi transport this step is performed by the TRAPP (transport protein particle) complex. The subunit Bet3 is present twice in the complex. It is thought that TRAPP performs its tethering function by interaction of Bet3 either with the vesicle's coat proteins or with the organelle membrane. The crystal structure of Bet3 shows a hydrophobic tunnel, in which a palmitate chain is embedded. The palmitate is covalently attached via a thioester bond to a fully conserved cysteine (C68) located at the entrance of the tunnel.

Several mechanisms for membrane binding of Bet3 have been suggested: the insertion of the covalently bound palmitoyl chain into the lipid bilayer of the membrane or the insertion of an acyl chain from a membrane lipid into the hydrophobic tunnel, and thirdly electrostatic binding via a positively charged patch on the Bet3 surface. Furthermore, binding could occur through interaction with a protein in the organelle membrane. Using LUVs (large unilamellar vesicles) as protein-free membrane models, it could be shown that no additional protein is needed to achieve transient membrane binding of human Bet3. Bet3 mutants without C68, with a blocked tunnel or without the positively charged patch all showed slightly reduced membrane binding, but neither mutation completely abolished it. It is therefore proposed that the binding of Bet3 is mediated by several weak interactions which in combination achieve a strong interaction force. In addition, the influence of membrane composition was investigated. Bet3 showed the strongest interaction with LUVs containing 10 % cholesterol whereas 40 % cholesterol strongly reduced membrane binding.

In the presence of palmitoyl-CoA Bet3 is acylated by an autocatalytic S_N2 mechanism at C68. Through a fluorescence quenching assay, it could be shown that Bet3 binds long chain fatty acid CoAs in micromolar range, whereas short chain fatty acid CoAs show only weak ligand binding in the millimolar range. In addition, three substrate binding sites have been identified: one inside the hydrophobic tunnel which is required for self-palmitoylation, and two additional hydrophobic patches located near the tunnel entrance on the protein surface. It is suggested that these external binding sites could help to extract Pal-CoA from the organelle membrane. Surface bound Pal-CoA might then be transferred into the tunnel by conformational change.

6.2 Zusammenfassung

In eukaryontischen Zellen erfolgt die Beförderung von Proteinen entlang sekretorischer und endozytischer Transportwege durch Membranvesikel. Der Erstkontakt zwischen Vesikel und Zielmembran wird durch sogenannte Tether vermittelt, im Falle das ER-Golgi-Transports durch den TRAPP (transport protein particle) Komplex. Die Untereinheit Bet3 kommt an beiden Enden des TRAPP Komplexes vor und erkennt auf der einen Seite die Vesikel durch Interaktion mit ihrem Proteinmantel, während es vermutlich gleichzeitig auf der anderen Seite den TRAPP Komplex an die Zielmembran bindet. Bet3 wird von einem hydrophoben Tunnel durchzogen, in welchem eine Palmitylfettsäure eingebettet ist. Diese ist über eine Thioesterbindung kovalent an ein konserviertes Cystein (C68) gebunden, welches am Tunneleingang lokalisiert ist.

Es wurden mehrere Mechanismen für die Membranbindung von Bet3 vorgeschlagen. Neben der Interaktion mit einem membranständigen Protein ist es denkbar, dass die Palmitylkette aus dem Tunnel herausklappt und sich in die Lipiddoppelschicht der Membran einlagert und/oder dass eine Fettsäurekette aus der Lipidschicht im hydrophoben Tunnel bindet. Desweitern verfügt Bet3 über einen positiv geladenen Bereich auf der Oberfläche, der über elektrostatische Wechselwirkung an die Membran binden könnte. Experimente mit LUVs (large unilamellar vesicles) als proteinfreien Membranmodellen zeigten, dass Bet3 dynamisch ohne die Mitwirkung eines zusätzlichen Proteins direkt an die Lipiddoppelschicht binden kann. Mutanten, in denen jeweils einer der genannten Bindungsmechanismen unterdrückt war, zeigten alle eine reduzierte Bindung. Jedoch konnte keine der Mutationen die Membranbindung vollständig unterbinden. Es ist daher anzunehmen, dass die Membranbindung durch die synergistische Verstärkung mehrerer schwacher Wechselwirkungen hervorgerufen wird. Zudem wurde der Einfluss der Membran-zusammensetzung untersucht. LUVs mit 10 % Cholesterol zeigten die stärkste Bindung, während bei LUVs mit 40 % Cholesterolgehalt die Membranbindung stark geschwächt war.

Bet3 wird durch Pamityl-CoA über einen autokatalytischen S_N2-Mechanismus an C68 acyliert. Mit Fluoreszenzquenchingexperimenten konnte gezeigt werden, dass langkettige Acyl-CoAs Bet3 im mikromolaren Bereich komplexieren, während kurzkettige Acyl-CoAs nur schwache Bindung im millimolaren Bereich zeigen. Zusätzlich wurden drei Substratbindungsstellen identifiziert. Eine ist der hydrophobe Tunnel, in welchen die Fettsäurekette einlagern muss, damit sie auf das Protein übertragen werden kann. Zwei weitere hydrophobe Bereiche wurden auf der Proteinoberfläche, nahe dem Tunneleingang, identifiziert. Möglicherweise, extrahieren diese Bindestellen Pal-CoA aus der Membran, welches dann durch eine Konformationsänderung in den Tunnel eingelagert wird.

7 Literature

1. Alberts, B., *Essential cell biology : an introduction to the molecular biology of the cell*. 1998, New York: Garland Pub.
2. Jones, S., et al., *The TRAPP complex is a nucleotide exchanger for Ypt1 and Ypt31/32.* Mol Biol Cell, 2000. **11**(12): p. 4403-11.
3. Wang, W., M. Sacher, and S. Ferro-Novick, *TRAPP stimulates guanine nucleotide exchange on Ypt1p.* J Cell Biol, 2000. **151**(2): p. 289-96.
4. Cai, Y., et al., *The structural basis for activation of the Rab Ypt1p by the TRAPP membrane-tethering complexes.* Cell, 2008. **133**(7): p. 1202-13.
5. Zerial, M. and H. McBride, *Rab proteins as membrane organizers.* Nat Rev Mol Cell Biol, 2001. **2**(2): p. 107-17.
6. Shorter, J., et al., *Sequential tethering of Golgins and catalysis of SNAREpin assembly by the vesicle-tethering protein p115.* J Cell Biol, 2002. **157**(1): p. 45-62.
7. Barrowman, J., M. Sacher, and S. Ferro-Novick, *TRAPP stably associates with the Golgi and is required for vesicle docking.* Embo j, 2000. **19**(5): p. 862-9.
8. Sacher, M., et al., *TRAPP I implicated in the specificity of tethering in ER-to-Golgi transport.* Mol Cell, 2001. **7**(2): p. 433-42.
9. Loh, E., et al., *Mammalian Bet3 functions as a cytosolic factor participating in transport from the ER to the Golgi apparatus.* J Cell Sci, 2005. **118**(Pt 6): p. 1209-22.
10. Yu, S., et al., *mBet3p is required for homotypic COPII vesicle tethering in mammalian cells.* J Cell Biol, 2006. **174**(3): p. 359-68.
11. Saraste, J., et al., *Emerging new roles of the pre-Golgi intermediate compartment in biosynthetic-secretory trafficking.* FEBS Lett, 2009. **583**(23): p. 3804-10.
12. Brunet, S. and M. Sacher, *In sickness and in health: the role of TRAPP and associated proteins in disease.* Traffic, 2014. **15**(8): p. 803-18.
13. Lynch-Day, M.A., et al., *Trs85 directs a Ypt1 GEF, TRAPPIII, to the phagophore to promote autophagy.* Proc Natl Acad Sci U S A, 2010. **107**(17): p. 7811-6.
14. Kim, J.J., Z. Lipatova, and N. Segev, *TRAPP Complexes in Secretion and Autophagy.* Front Cell Dev Biol, 2016. **4**: p. 20.
15. Sacher, M., et al., *TRAPP, a highly conserved novel complex on the cis-Golgi that mediates vesicle docking and fusion.* Embo J, 1998. **17**(9): p. 2494-503.
16. Turnbull, A.P., et al., *Structure of palmitoylated BET3: insights into TRAPP complex assembly and membrane localization.* Embo J, 2005. **24**(5): p. 875-84.
17. Kim, Y.G., et al., *Crystal structure of bet3 reveals a novel mechanism for Golgi localization of tethering factor TRAPP.* Nat Struct Mol Biol, 2005. **12**(1): p. 38-45.
18. Kümmel, D., U. Heinemann, and M. Veit, *Unique self-palmitoylation activity of the transport protein particle component Bet3: a mechanism required for protein stability.* Proc Natl Acad Sci U S A, 2006. **103**(34): p. 12701-6.
19. Bijlmakers, M.J. and M. Marsh, *The on-off story of protein palmitoylation.* Trends Cell Biol, 2003. **13**(1): p. 32-42.
20. Linder, M.E. and R.J. Deschenes, *Palmitoylation: policing protein stability and traffic.* Nat Rev Mol Cell Biol, 2007. **8**(1): p. 74-84.
21. Roth, A.F., et al., *The yeast DHHC cysteine-rich domain protein Akr1p is a palmitoyl transferase.* J Cell Biol, 2002. **159**(1): p. 23-8.
22. Jennings, B.C. and M.E. Linder, *DHHC protein S-acyltransferases use similar ping-pong kinetic mechanisms but display different acyl-CoA specificities.* J Biol Chem, 2012. **287**(10): p. 7236-45.
23. Roth, A.F., et al., *Global analysis of protein palmitoylation in yeast.* Cell, 2006. **125**(5): p. 1003-13.

24. Faergeman, N.J. and J. Knudsen, *Role of long-chain fatty acyl-CoA esters in the regulation of metabolism and in cell signalling.* Biochem J, 1997. **323 (Pt 1)**: p. 1-12.
25. Kümmel, D., et al., *Characterization of the self-palmitoylation activity of the transport protein particle component Bet3.* Cell Mol Life Sci, 2010. **67**(15): p. 2653-64.
26. Lakowicz, J.R., *Principles of fluorescence spectroscopy*. 3rd ed. 2006, New York: Springer. p. 356-357. The theoretical basis for the introductary chapter about fluorescence has been gained from this book.
27. Laemmli, U.K., *Cleavage of structural proteins during the assembly of the head of bacteriophage T4.* Nature, 1970. **227**(5259): p. 680-5.
28. De Blas, A.L. and H.M. Cherwinski, *Detection of antigens on nitrocellulose paper immunoblots with monoclonal antibodies.* Anal Biochem, 1983. **133**(1): p. 214-9.
29. Urban, A., S. Neukirchen, and K.E. Jaeger, *A rapid and efficient method for site-directed mutagenesis using one-step overlap extension PCR.* Nucleic Acids Res, 1997. **25**(11): p. 2227-8.
30. Veit, M., E. Ponimaskin, and M.F. Schmidt, *Analysis of S-acylation of proteins.* Methods Mol Biol, 2008. **446**: p. 163-82.
31. Heck, M. and K.P. Hofmann, *G-protein-effector coupling: a real-time light-scattering assay for transducin-phosphodiesterase interaction.* Biochemistry, 1993. **32**(32): p. 8220-7.
32. Duncan, J.A. and A.G. Gilman, *Autoacylation of G protein alpha subunits.* J Biol Chem, 1996. **271**(38): p. 23594-600.
33. Thaa, B., A. Herrmann, and M. Veit, *The polybasic region is not essential for membrane binding of the matrix protein M1 of influenza virus.* Virology, 2009. **383**(1): p. 150-5.
34. Zambrano, F., S. Fleischer, and B. Fleischer, *Lipid composition of the Golgi apparatus of rat kidney and liver in comparison with other subcellular organelles.* Biochim Biophys Acta, 1975. **380**(3): p. 357-69.
35. van Meer, G. and A.I. de Kroon, *Lipid map of the mammalian cell.* J Cell Sci, 2011. **124**(Pt 1): p. 5-8.
36. van Meer, G., D.R. Voelker, and G.W. Feigenson, *Membrane lipids: where they are and how they behave.* Nat Rev Mol Cell Biol, 2008. **9**(2): p. 112-24.
37. Mouritsen, O.G. and M.J. Zuckermann, *What's so special about cholesterol?* Lipids, 2004. **39**(11): p. 1101-13.
38. Ingolfsson, H.I., et al., *Lipid organization of the plasma membrane.* J Am Chem Soc, 2014. **136**(41): p. 14554-9.
39. Resh, M.D., *Use of analogs and inhibitors to study the functional significance of protein palmitoylation.* Methods, 2006. **40**(2): p. 191-7.
40. Levental, I., M. Grzybek, and K. Simons, *Greasing their way: lipid modifications determine protein association with membrane rafts.* Biochemistry, 2010. **49**(30): p. 6305-16.
41. Levental, I., et al., *Palmitoylation regulates raft affinity for the majority of integral raft proteins.* Proc Natl Acad Sci U S A, 2010. **107**(51): p. 22050-4.
42. Abrami, L., S.H. Leppla, and F.G. van der Goot, *Receptor palmitoylation and ubiquitination regulate anthrax toxin endocytosis.* J Cell Biol, 2006. **172**(2): p. 309-20.
43. Li, H. and V. Papadopoulos, *Peripheral-type benzodiazepine receptor function in cholesterol transport. Identification of a putative cholesterol recognition/interaction amino acid sequence and consensus pattern.* Endocrinology, 1998. **139**(12): p. 4991-7.
44. Azarashvili, T., et al., *Effect of the CRAC Peptide, VLNYYVW, on mPTP Opening in Rat Brain and Liver Mitochondria.* Int J Mol Sci, 2016. **17**(12).
45. Posada, I.M., et al., *A cholesterol recognition motif in human phospholipid scramblase 1.* Biophys J, 2014. **107**(6): p. 1383-92.
46. Fantini, J. and F.J. Barrantes, *How cholesterol interacts with membrane proteins: an exploration of cholesterol-binding sites including CRAC, CARC, and tilted domains.* Front Physiol, 2013. **4**: p. 31.

47. Mukai, M., M.R. Krause, and S.L. Regen, *Peptide Recognition of Cholesterol in Fluid Phospholipid Bilayers.* J Am Chem Soc, 2015. **137**(39): p. 12518-20.
48. Linder, M.E. and B.C. Jennings, *Mechanism and function of DHHC S-acyltransferases.* Biochem Soc Trans, 2013. **41**(1): p. 29-34.
49. Vance, J.E., *Phospholipid synthesis and transport in mammalian cells.* Traffic, 2015. **16**(1): p. 1-18.
50. Lerche, M.H., et al., *Barley lipid-transfer protein complexed with palmitoyl CoA: the structure reveals a hydrophobic binding site that can expand to fit both large and small lipid-like ligands.* Structure, 1997. **5**(2): p. 291-306.
51. Lerche, M.H. and F.M. Poulsen, *Solution structure of barley lipid transfer protein complexed with palmitate. Two different binding modes of palmitate in the homologous maize and barley nonspecific lipid transfer proteins.* Protein Sci, 1998. **7**(12): p. 2490-8.
52. Hamilton, J.A., *Fatty acid interactions with proteins: what X-ray crystal and NMR solution structures tell us.* Prog Lipid Res, 2004. **43**(3): p. 177-99.

8 Publication

Parts of this dissertation have been published in:

Kümmel, D., Walter, J., Heck, M., Heinemann, U., Veit, M., *Characterization of the self-palmitoylation activity of the transport protein particle component Bet3.* Cell Mol Life Sci, 2010. **67**(15): p. 2653-64

9 Appendix

9.1 Vector maps

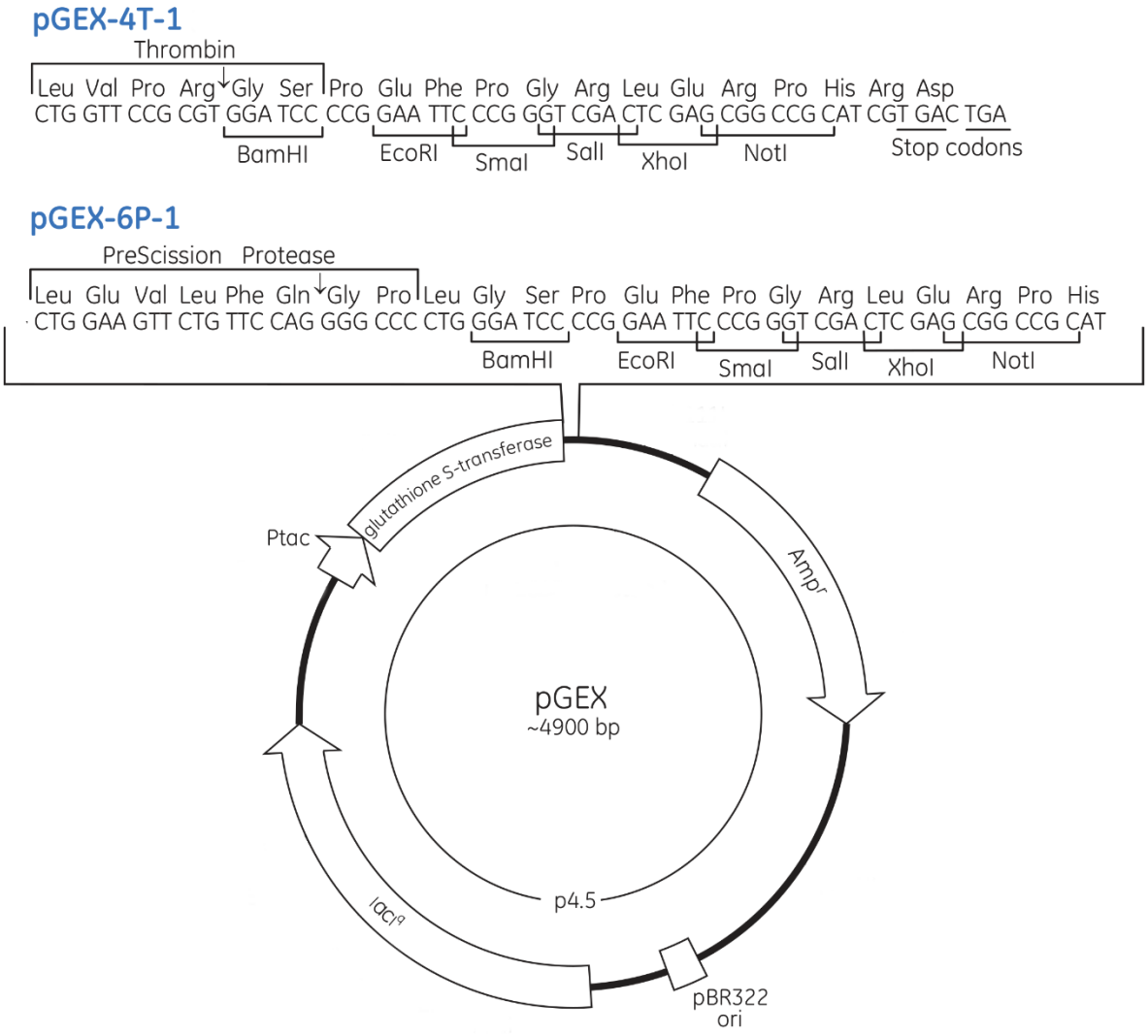

Figure 9.1: Maps of the vectors pGex-4T-1 and pGex-6P-1. Graphic adapted from the GST gene fusion system handbook (GE Healthcare).

The protein expression is under control of a *tac* promoter which is induced by the lactose analog isopropyl β-D-thiogalactoside (IPTG). The plasmid also carries an ampicillin resistance to allow for the selection of successfully transformed bacteria. The protein is expressed fused with a GST tag in front. The tag can be removed with thrombin in case of pGex-4T-1 and PreScission Protease in case of pGex-6P-1.

9.2 Mathematical description of fluorescence anisotropy

The fluorescence anisotropy (r) is given through the ratio of the intensity of vertical polarized emission to total emission:

$$r = \frac{I_{\parallel} - I_{\perp}}{I_{\parallel} + 2I_{\perp}} \tag{9.2.1}$$

$I_{\parallel}$: intensity of emission parallel, $I_{\perp}$: Intensity of emission horizontal to the excitation polarization plane.

To deduce a mathematical description of fluorescence anisotropy one starts with the emission of a single, immobilized fluorophore with parallel dipole transition moments. The orientation of the dipole is described by a coordinate system whose x-axis is parallel to the direction of the incoming light beam, the z-axis parallel to the excitation polarization plane and the y-axis the direction of emission detection (see fig. 9.2 A).

The total emission equals $I_{\parallel} + 2I_{\perp}$, because if the excitation polarization is parallel to e.g. the z-axis, the horizontal emission along y- as well as x-axis has to be added to obtain the total intensity of emission. Hence the anisotropy of a single, stationary fluorophore is r = 1, provided the transition dipole moments of excitation and emission are parallel.

θ is the angle between emission dipole and excitation polarization plane, ϕ the angle of the dipole's rotation around the z-axis.

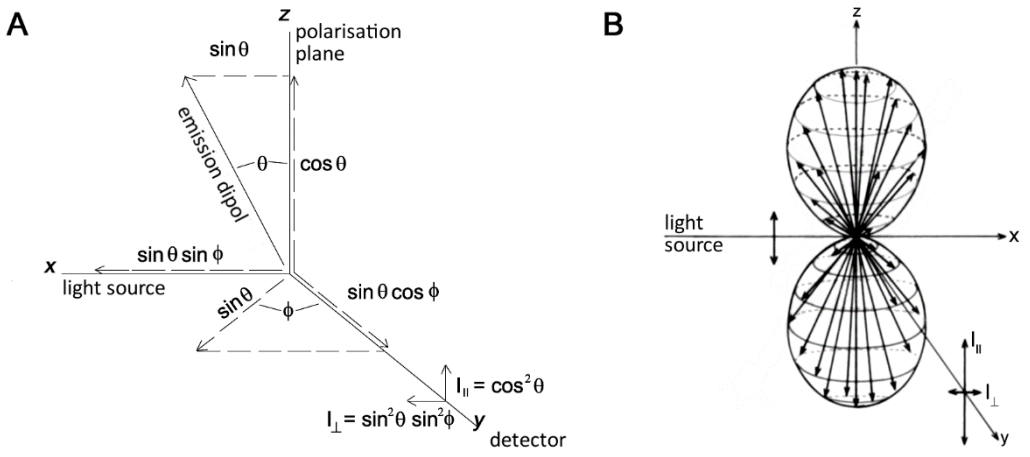

(adapted from Lakowicz, J.R., Principles of fluorescence spectroscopy. 2006)

Figure 9.2: (A) Emission intensities of a single fluorophore in a coordinate system. (B) Distribution of excited states for a single, immobilized fluorophore [26].

When the emission is detected with polarization filters horizontal ($I_{\parallel}$) and vertical ($I_{\perp}$) to the excitation polarization plane, the intensity can be described in dependence of θ and ϕ as:

$$I_{\parallel}(\theta,\phi) = \cos^2\theta \quad \text{and} \quad I_{\perp}(\theta,\phi) = \sin^2\theta \sin^2\phi \tag{9.2.2}$$

In a sample with randomly oriented fluorophores, it can be assumed that all fluorophores which are oriented towards the excitation polarization plane in the same angle θ are excited with equal probability (photo selection). In consequence the emitting fluorophores will be equally distributed in an angle ϕ between 0 and 2π around the z-axis (see fig. 9.2 B). The term $\sin^2\phi$ can therefore be replaced with the average value of $\sin^2\phi$ given by:

$$\langle \sin^2\phi \rangle = \frac{\int_0^{2\pi} \sin^2\phi d\phi}{\int_0^{2\pi} d\phi} = \frac{1}{2} \tag{9.2.3}$$

Thus the emission intensities can be expressed as:

$$I_{\parallel}(\theta) = \cos^2\theta \quad \text{and} \quad I_{\perp}(\theta) = \frac{1}{2}\sin^2\theta \tag{9.2.4}$$

To fully describe freely rotating fluorophores one has also to consider the probability that a fluorophore orientated towards the z-axis in a given angle θ is excited. The excitation dipole does not need to be exactly aligned parallel to the polarization plane, rather the probability of excitation can be described as proportional to $\cos^2\theta$. The probability of excitation can be visualized as a "dumbbell" oriented along the z-axis (see fig. 9.2 B). Thus the entirety of excited fluorophores depends on the average distribution of excitation dipoles between θ = 0 and π/2:

$$I_{\parallel}(\theta) = \langle \cos^2\theta \rangle \quad \text{and} \quad I_{\perp}(\theta) = \frac{1}{2}\langle \sin^2\theta \rangle \tag{9.2.5}$$

By insertion of equation 9.2.5 and $\sin^2 = \cos^2 - 1$ in equation 9.2.1 one derives the following expression:

$$r = \frac{3\langle \cos^2\theta \rangle - 1}{2} \tag{9.2.6}$$

The average distribution of excitation dipoles between $\theta = 0$ and $\pi/2$ is described by:

$$\langle \cos^2 \theta \rangle = \frac{\int_0^{\pi/2} \cos^2\theta \, d\theta}{\int_0^{\pi/2} d\theta} = \frac{3}{5} \tag{9.2.7}$$

Hence the maximum anisotropy of randomly distributed fluorophores in solution cannot exceed r = 0.4. Higher anisotropy values indicate light scattering due to e.g. turbidity of the sample.

Many fluorophores have excitation and emission transition moments which are not parallel. The relative angular displacement (β) between them also lowers the observed anisotropy values. This can be described in analogy to the orientation to the z-axis with the factor $(3\cos^2\beta\text{-}1)/2$, which then has to be multiplied by 2/5 stemming from the loss of anisotropy due to photoselection. Hence the maximal anisotropy value of a given fluorophore solution (r_0) is given as:

$$r_0 = \frac{2}{5}\left(\frac{3\cos^2\beta - 1}{2}\right) \tag{9.2.8}$$

Depending on the angle between the transition moments, r_0 can range between 0.4 (β = 0°) and -0.2 (β = 90°).

For practical purposes the instrumental error also has to be taken into account. It is largely due to a wavelength dependency of the emission monochromator. Monochromators transmit light with varying sensitivity (S) depending on wavelength and orientation of the polarization plane. The dependence of the measured intensities on the monochromator sensitivity can be expressed as:

$$I_{VV} = S_V I_{\parallel} \quad \text{and} \quad I_{VH} = S_H I_{\perp} \tag{9.2.9}$$

The connotations indicate the polarizer orientation, e.g. I_{VH} excitation vertical emission horizontal. The ratio of the measured intensities (I_{VV} and I_{VH}) is therefore proportional to the true intensities ($I_{\parallel}$ and $I_{\perp}$). They differ by the instrumental factor G which expresses the ratio of the polarization-dependent sensitivity.

$$\frac{I_{VV}}{I_{VH}} = \frac{S_V I_{\parallel}}{S_H I_{\perp}} = G\frac{I_{\parallel}}{I_{\perp}} \tag{9.2.10}$$

The G factor can easily be determined by measuring with the excitation polarizer in horizontal position, so that the transition moment of excited fluorophores is oriented parallel to the direction of detection. Then with horizontal (I_{HH}) and vertical (I_{HV}) orientation of the emission polarizer only the horizontal component of the emission intensity ($I_{\perp}$) is detected (see fig. 1.6).

$$\frac{I_{HV}}{I_{HH}} = \frac{S_V I_{\perp}}{S_H I_{\perp}} = \frac{S_V}{S_H} = G \tag{9.2.11}$$

If equation 9.2.11 is solved for $I_{\parallel}$ and $I_{\perp}$ and inserted into equation 9.2.1 the anisotropy is given by:

$$r = \frac{I_{VV} - G I_{VH}}{I_{VV} + 2G I_{VH}} \tag{9.2.12}$$

This equation can then be used to calculate the fluorescence anisotropy from the measured intensities.

9.3 Deduction of the equation for analysis of the fluorescence quenching assay

The mathematical model to calculate the K_D value and the number of acyl-CoA binding sites of Bet3 is based on a bimolecular reaction with depletion of both reactants. The total concentration of ligand binding sites in the assay equals the protein concentration times the number of ligand binding sites per protein molecule. The binding of acyl-CoAs to Bet3 can then be viewed as a bimolecular reaction between ligand and binding site:

$$L + nP = nPL \quad \text{with the kinetic given as} \quad [nPL] = \frac{1}{K_D}[nP][L] \tag{9.3.1}$$

The concentration of free reactant can be expressed as:

$$[nP] = [nP]_{tot} - [nPL] \quad \text{and} \quad [L] = [L]_{tot} - [nPL] \tag{9.3.2}$$

Therefore, the concentration of complexed binding sites can be described as:

$$[nPL] = \frac{1}{K_D}([nP]_{tot} - [nPL])([L]_{tot} - [nPL]) \tag{9.3.3}$$

After rearranging, the quadratic equation can be solved.

$$[nPL] = \frac{1}{K_D}\left([nPL]^2 + [nPL](-[nP]_{tot} - [L]_{tot}) + ([L]_{tot}[nP]_{tot})\right)$$

$$K_D[nPL] = [nPL]^2 - [nPL]([nP]_{tot} + [L]_{tot} + K_D) + ([L]_{tot}[nP]_{tot})$$

$$0 = K_D[nPL] = [nPL]^2 - [nPL]([nP]_{tot} + [L]_{tot} + K_D) + ([L]_{tot}[nP]_{tot})$$

$$[nPL] = \frac{-([nP]_{tot}+[L]_{tot}+K_D)-\sqrt{([nP]_{tot}+[L]_{tot}+K_D)^2-4([L]_{tot}[nP]_{tot})}}{2} \quad (9.3.4)$$

The proportion of change in fluorescence intensity (Y) to maximal fluorescence intensity (Y_{max}) equals the proportion of complexed binding sites complex to the total amount of binding sites.

$$\frac{Y}{Y_{max}} = \frac{[nPL]}{[nP]} \quad (9.3.5)$$

With the total concentration of ligand $[L]_{tot}$ and protein binding sites $[nP]_{tot}$ abbreviated to L and nP the change in fluorescence intensity can thus be described by:

$$\mathrm{Y} = \frac{-(\mathrm{nP}+\mathrm{L}+K_D)-\sqrt{(\mathrm{nP}+\mathrm{L}+K_D)^2-4\mathrm{LnP}}}{2\mathrm{nP}/\,Y_{max}} \quad (9.3.6)$$

K_D: apparent dissociation constant for acyl-CoA, L/P: ligand/protein concentration, n: number of ligand binding sites per protein and Y_{max}: maximal change in fluorescence intensity.

9.4 Abbreviations

µM	micromolar
ACBP	acyl-CoA binding protein
Ac-CoA	acetyl-CoA
CD	circular dichroism
Chol	cholesterol
COPII	coat protein complex II
CRAC	cholesterol recognition/interaction amino acid consensus
ER	endoplasmic reticulum
GEF	guanidine exchange factor
GST	glutathione *S*-transferase
HA	influenza hemagglutinin
IC	intermediate compartment
KD	dissociation constant
KM	Michaelis constant
LM	lipid mix
LTP	lipid transfer protein
LUV	large unilamellar vesicles
mM	millimolar
Myr-CoA	myristoyl-CoA
Myr-X-CoA	non-hydrolysable myristoyl-CoA thioether
NBD-PC	N-(7-nitro-2-3,1-benzooxadiazol-4-yl)dioleyl-phosphatidylcholine (fluorescent)
NMR	nuclear magnetic resonance
Oct-CoA	octanoyl-CoA
Ol-CoA	oleoyl-CoA
Pal-CoA	palmitoyl-CoA
PC	phosphatidylcholine
PCR	polymerase chain reaction
PE	phosphatidylethanolamine
pH	potential of hydrogen
PI	phosphatidylinositol
pK_a	acid dissociation constant
PS	phosphatidylserin
r	anisotropy
S_N2	bimolecular nucleophilic substitution
SNARE	soluble N-ethylmaleimide-sensitive-factor attachment receptor
Stear-CoA	stearoyl-CoA
SUV	small unilamellar vesicles
TRAPP	transport protein particle
WT	wildtype